Since January 2020 Elsevier has created a COVID-19 resource centre with free information in English and Mandarin on the novel coronavirus COVID-19. The COVID-19 resource centre is hosted on Elsevier Connect, the company's public news and information website.

International Journal of Pharmaceutics 609 (2021) 121113

Contents lists available at ScienceDirect

International Journal of Pharmaceutics

journal homepage: www.elsevier.com/locate/ijpharm

Advancing insights on β-cyclodextrin inclusion complexes with SSRIs through lens of X-ray diffraction and DFT calculation

Thammarat Aree

Department of Chemistry, Faculty of Science, Chulalongkorn University, Bangkok 10330, Thailand

ARTICLE INFO

Keywords:
β-Cyclodextrin
Fluoxetine
Paroxetine
Sertraline
X-ray analysis
DFT calculation

ABSTRACT

Depression—the global crisis hastened by the coronavirus outbreak, can be efficaciously treated by the selective serotonin reuptake inhibitors (SSRIs). Cyclodextrin (CD) inclusion complexation is a method of choice for reducing side effects and improving bioavailability of drugs. Here, we investigate in-depth the β-CD encapsulation of sertraline (STL) HCl (**1**) and fluoxetine (FXT) HCl (**2**) by single-crystal X-ray diffraction and DFT complete-geometry optimization, in comparison to the reported complex of paroxetine (PXT) base. X-ray analysis unveiled the 2:2 β-CD–STL/FXT complexes with two drug molecules inserting their halogen-containing aromatic ring in the β-CD dimeric cavity, which are stabilized by the interplay of intermolecular O2–H···N1–H···O3 H-bonds, C3/C5–H···π and halogen···halogen interactions. Similarly, the 1:1 β-CD–tricyclic-antidepressant (TCA) complexes have an exclusive inclusion mode of the aromatic ring, which is maintained by C3/C5–H···π interactions. By contrast, the 2:1 β-CD–PXT complex has a total inclusion that is stabilized by host–guest O6–H···N1–H···O5 H-bonds and C3–H···π interactions. The inherent stabilization energies of **1** and **2** evaluated using DFT calculation suggested that the improved thermodynamic stabilities via CD encapsulation facilitates the reduction of drug side effects. Moreover, the SSRI conformational flexibilities are thoroughly discussed for understanding of their pharmacoactivity.

1. Introduction

Depression is a global mental illness as over 300 million people suffer from it and about 800,000 people die from suicide each year (WHO, 2017) – the situation before the coronavirus disease 2019 (COVID-19) pandemic. Recent data of the COVID-19 era frighten us: i) 1.5-year since the outbreak, the number of confirmed COVID-19 cases has gone beyond 170 million worldwide (Our World in Data, 2021); ii) about one-fourth of COVID-19 patients globally commonly experience depression (Rogers et al., 2021); and iii) one-half of the COVID-19 survivors suffer from depression (Perlis et al., 2021). An efficacious treatment for depression is achievable by using antidepressants. Selective serotonin reuptake inhibitors (SSRIs) are first-line, second-generation antidepressants including for example, sertraline (STL; Zoloft), fluoxetine (FXT; Prozac) and paroxetine (PXT; Paxil), Scheme 1. SSRIs for the treatment of depression have been approved by the US Food and Drug Administration (FDA, 2014). Prozac is one of the most commonly prescribed and popular SSRIs in the US (Stokes and Holtz, 1997) as it is the only FDA-approved drug for adolescents (McClanahan, 2009). SSRIs have equivalent clinical efficacy in treating depression to tricyclic antidepressants (TCAs), first-generation drugs, and have fewer side effects due to their high selectivity in binding with serotonin transporters. Hence, SSRIs are safer in overdose than TCAs (Peretti et al., 2000). SSRI drugs are rather less soluble in water and hence have limited oral bioavailability. To overcome the problem, the cyclodextrin encapsulation is a method of choice for enhancing aqueous solubility and reducing side effects of SSRIs (Passos et al., 2011, 2012; Buko et al., 2017; Abouhussein et al., 2019). Plus, light in the mist of COVID-19 crisis, SSRIs with anti-inflammatory properties can be used in treating COVID-19-associated inflammatory lung disease, thus reducing severity of COVID-19 (Lenze et al., 2020; Hoertel et al., 2021; Meikle et al., 2021).

α-, β-, γ-Cyclodexrins (CDs) are versatile encapsulating agents comprising 6, 7, 8 D-glucose units, respectively. CDs adopt a shape of hollow, truncated cone and are amphiphilic with hydrophobic central cavity and hydrophilic rims (Scheme 1). They can accommodate a variety of guest molecules fitting partly or wholly to their apolar cavity, yielding inclusion complexes (Dodziuk, 2006). The host–guest supramolecular complexes are stabilized by noncovalent intermolecular interactions, e.g., hydrogen bonds, hydrophobic and van der Waals interactions. The CD encapsulation has various practical applications

E-mail address: athammar@chula.ac.th.

https://doi.org/10.1016/j.ijpharm.2021.121113
Received 30 July 2021; Received in revised form 2 September 2021; Accepted 15 September 2021
Available online 20 September 2021

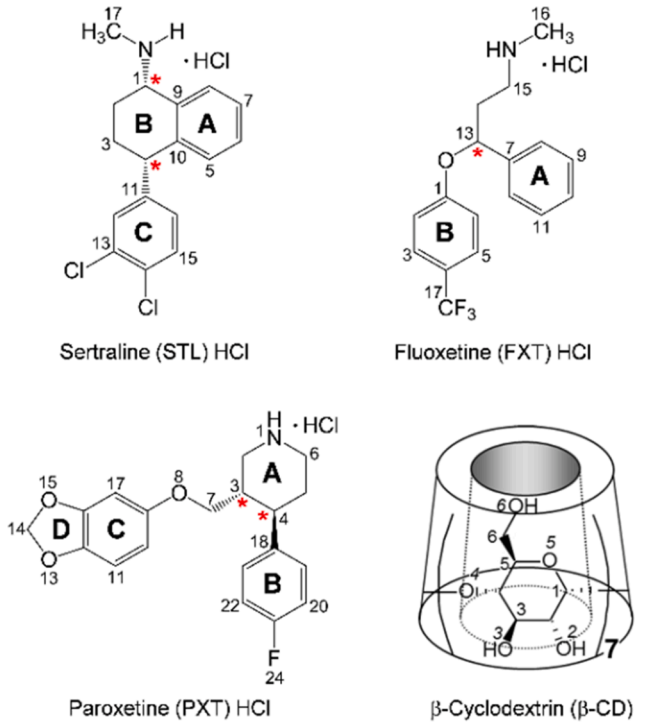

Scheme 1. Chemical structures and atom numbering schemes of SSRIs (STL, FXT and PXT) and β-CD; the A-, B-, C-, D-rings and chiral centers of SSRIs are also marked. The commercially available forms of SSRIs are (1*S*,4*S*)-STL HCl diastereomer, racemate FXT HCl and (3*S*,4*R*)-PXT HCl. Note that the (*R*)- and (*S*)-enantiomers of FXT have equivalent SSRI activity (Wong et al., 1985).

including pharmaceutics, cosmetics, medicine, food, chromatography, biotechnology, and nanotechnology (Adeoye and Cabral-Marques, 2017; Bakshi and Londhe, 2020; Fourmentin et al., 2018; Liu et al., 2020; Morin-Crini et al., 2021). In pharmaceutical technology, CD inclusion complexation improves the physicochemical and pharmacological properties of drugs; see a recent patent review for antidepressants (Diniz et al., 2018). Here, we provide an insightful literature review of the CD–SSRI inclusion complexes, focusing on STL, FXT and PXT. These SSRIs are less structurally similar, but commonly contain halogens relating to their serotonin reuptake efficacy. Considerable research attention has been paid to the CD–STL/FXT/PXT inclusion complexes over the past 20 years.

The CD encapsulation of STL is the most studied among the SSRIs. The 2:1 and 1:1 β-CD–STL HCl complexes are in equilibrium with the tetrahydronaphthalene (A–B-rings), dichlorophenyl (C-ring) and methylamine moieties embedded in the CD cavities, and the DFT-derived stabilization energies are −12.7 and −14.5 kcal mol^{-1}, respectively (Passos et al., 2011). The stable equimolar β-CD–STL HCl complex with an association constant (K_a) of 4999 ± 495 M^{-1} as determined by isothermal titration calorimetry (ITC) (Passos et al., 2011, 2013) helped to improve the drug solubility and transport efficacy in vivo (Passos et al., 2012). Thermodynamic properties of the 1:1 complex with the STL methylamine portion entering the β-CD O2–H/O3–H-side as derived from DFT calculation in the explicit hydration water agree with experimental data (Lopes et al., 2015). NMR, UV–vis, and ITC data revealed that both β-CD and dimethyl-β-CD (DIMEB) form 1:1 complexes with STL HCl with K_a's in the respective ranges of 5300–5850 ± 500 and 7960–8600 ± 500 M^{-1} (Belica et al., 2014). The greater K_a's of DIMEB complexes over those of β-CD complexes are due to the better fit of STL aromatic portion to the more hydrophobic DIMEB cavity (Belica et al., 2014). Moreover, the pharmacological activity of STL HCl is improved via equimolar complexation with hydroxypropyl-β-CD (HP-β-CD) with K_a = 6530 ± 54 M^{-1} from ITC (Buko et al., 2017).

In the solid state, NMR data indicated the stable 1:1 β-CD–STL base complex with the A–B-rings partially entrapped in the β-CD cavity and K_a = 4300 M^{-1}, based on the vibrational spectra (IR, Raman) and phase solubility data, respectively (Ogawa et al., 2015). Recently, sublingual orodispersible tablet formulated from the β-CD–STL solid dispersion enhanced the STL dissolution and rapid absorption through the oral mucosa, thus improving the drug bioavailability (Abouhussein et al., 2019).

The CD–FXT complexes draw attention to some extent. FXT HCl embedded in the γ-CD cavity increased the drug pharmacological efficacy (Géczy et al., 2000). Ali et al. (2005) inferred from NMR data the 1:1 β-CD–FXT HCl inclusion complex with rather low and underestimated K_a of ~ 70 M^{-1}. The trifluorotoluene B-ring is enclosed in the β-CD cavity and the CF_3 group is protruded from the O6–H side, establishing O6–H···F H-bond and thus stabilizing the inclusion complex (Ali et al., 2005). The host–guest stoichiometry and inclusion structure of the β-CD–FXT HCl complex have been confirmed by NMR combined with DFT calculation, and the K_a value deduced from ITC seems more reasonable, 6921 ± 316 M^{-1} (de Sousa et al., 2008).

The β-CD encapsulation of PXT received less attention compared to other complexes. In solution, NMR combined with molecular dynamics (MD) simulation suggested the 1:1 β-CD–PXT base inclusion complex is quite stable with K_a ~ 2000 M^{-1} (Bernini et al., 2004). The corresponding inclusion structure is that the benzodioxole (C–D-ring) moiety is deeply inserted in the β-CD cavity and the fluorophenyl B-ring is outside the cavity nearby the O2–H/O3–H side (Bernini et al., 2004). On the contrary, in the solid state where intermolecular interactions between CD molecules are present, the apparent host–guest molar ratio is 2:1 (Caira et al., 2003). PXT base is totally entrapped in the head-to-head β-CD dimer such that the piperidine A-ring is nearby the O6–H side of one β-CD monomer, whereas the B-ring and C–D-ring moieties respectively reside in the dimer interfacial region and the cavity of another β-CD monomer (Caira et al., 2003).

CDs are non-toxic, biodegradable, and biocompatible (Del Valle, 2004). Among them, β-CD is the most studied because of its lower price and more optimum cavity size for harboring various guest molecules containing aromatic ring(s). This is evidenced by the predominant number of reported β-CD structures deposited to the Cambridge Crystallographic Data Centre (CCDC) (Groom et al., 2016). As thoroughly reviewed above, the atomic-level characteristics of β-CD–SSRI complexes (i.e., the inclusion structures and the host–guest stoichiometric ratios) remain rather controversial and deserve a comprehensive structural investigation. Because the SSRI drugs have varied structural moieties including the five-, six-membered rings and the side chain, hence this study has a twofold hypothesis. i) Among different SSRI structural moieties, the halogen-bearing aromatic ring provides better fit to the β-CD nanocavity for thermodynamically favorable inclusion complexation that is stabilized by optimal host–guest interactions. ii) SSRIs conformational flexibility in different lattice environments (in free salt form, in the CD cavity and in complex with proteins), is correlated with their pharmaceutical activity. To prove the two hypotheses, we carry out single-crystal X-ray diffraction and DFT full-geometry optimization of the β-CD encapsulation of STL and FXT. Because PXT is rather bulkier than other SSRIs and it shares a structural motif of an aryloxypropylamine with FXT, we make detailed structural comparisons of the β-CD–STL and β-CD–FXT complexes with the β-CD–PXT complex (Caira et al., 2003) and of STL, FXT and PXT in three distinct circumstances.

2. Materials and methods

2.1. Materials

β-CD (≥95%) was purchased from Cyclolab, Budapest, Hungary (code CY-2001). (1*S*,4*S*)-STL HCl (≥98%) and *rac*-FXT HCl (≥98%) were supplied by TCI Chemicals (codes S0507 and F0750). Absolute EtOH (≥99.8%) was provided by Liquor Distillery Organization, Excise

Department, Thailand. All chemicals were used as received. The ultrapure water was obtained from a Milli-Q Water System.

2.2. X-ray crystallography

2.2.1. Single-crystal preparation

Homogeneous, concentrated equimolar solutions of the β-CD–STL HCl (**1**) and β-CD–FXT HCl (**2**) inclusion complexes were prepared by dissolving the solid powders of β-CD 50 mg (0.044 mmol), STL HCl 15.1 mg (0.044 mmol) and FXT HCl 15.2 mg (0.044 mmol) in 1 mL of 50% (v/v) EtOH–H_2O at 323 K. The vials containing solutions of both complexes were left standing still in an air-conditioned room (298 K). After two weeks of slow solvent evaporation, single crystals for X-ray analysis were harvested.

2.2.2. X-ray diffraction experiment

Colorless rod-shaped single crystals of **1** and **2** were separately mounted in a thin-walled glass capillary (Hilgenberg, Germany). For both complexes, several crystals were checked for consistent unit cell constants and sufficient diffracting power. Different specimens crystallizing in the triclinic system with similar unit cell parameters provide strong evidence of a given inclusion complex. The best diffracting crystals of **1** and **2** were chosen for X-ray data collection at 296 K to 0.83-Å atomic resolution on a Bruker APEXII CCD area-detector diffractometer (MoKα radiation; $\lambda = 0.71073$ Å). Data processing assisted by the APEX2 software suite (Bruker, 2014) was accomplished according to standard procedures, i.e., began with integration using SAINT (Bruker, 2008), followed by scaling and multi-scan absorption correction using SADABS (Bruker, 2014), and completed by merging with XPREP (Bruker, 2008). The total numbers of 30,769 and 33,629 independent reflections with R_{int} of 0.0488 and 0.0518 for the respective complexes **1** and **2** were obtained.

2.2.3. Structure solution and refinement

The crystal structures of **1** and **2** were solved by intrinsic phasing method with SHELXTL XT (Bruker, 2014), providing all non-H atoms of β-CD dimers, STL, and most non-H atoms of FXT molecules. The missing non-H atoms of FXT were located by difference Fourier electron density maps graphically assisted by WinCoot (Emsley et al., 2010). Then a number of restraints were applied to FXT during the refinement. In the β-CD dimeric cavity of **1** and **2**, the occupancy factors of two STL and two FXT sites, each was refined to unity, yielding 2:2 host–guest complexes. The protonated STL and FXT molecules were counterbalanced and indirectly coordinated by doubly disordered chlorides, which were previously observed in the crystals of eight β-CD–TCA HCl inclusion complexes (Aree, 2020a, 2020b, 2020c, 2021).

The rest of non-H atoms including water O atoms and chloride ions were located by difference Fourier maps. Most of non-H atoms were refined anisotropically by full-matrix least-squares on F^2 using SHELXTL XLMP (Bruker, 2014), except for some O6–H groups of β-CD (**2**), two FXT (**2**) and disordered water molecules, which were refined isotropically. H atoms of rigid groups were positioned geometrically and treated with a riding model: C−H = 0.93 Å, $U_{iso} = 1.2U_{eq}$(C)(aromatic); C−H = 0.98 Å, $U_{iso} = 1.2U_{eq}$(C)(methine); C−H = 0.97 Å, $U_{iso} = 1.2U_{eq}$(C)(methylene); C−H = 0.96 Å, $U_{iso} = 1.5U_{eq}$(C)(methyl); and N−H = 0.89 Å, $U_{iso} = 1.2U_{eq}$(2° ammonium). The hydroxyl H-atoms initially located by difference Fourier maps were refined using ′AFIX 147′ or ′AFIX 83′ with restraints O−H = 0.84 Å, $U_{iso} = 1.5U_{eq}$(O). Water H-atoms could not be located by difference Fourier maps. To prevent short H•••H distances in the refinement, BUMP antibumping restraints were applied. The refinement of **1** converged to a final $R_1 = 0.0855$. For **2**, 27.4 water molecules were spread over 50 sites outside the β-CD dimeric cavity, filling in the intermolecular interstices. Most water sites were not in hydrogen bonding contact with β-CD or FXT molecules. Therefore, all water sites as large solvent voids were removed from the structure model in the final refinement using the PLATON SQUEEZE procedure (Spek, 2015), yielding $R_1 = 0.1035$, which was improved by 0.0252. For more details of data collection and refinement statistics, see Supplementary material, Table S1.

2.3. DFT full-geometry optimization

Accurately determined X-ray structures are good sources of initial atomic coordinates for DFT complete-geometry optimization of the supramolecular CD inclusion complexes, of which CDs are conformationally flexible. This has been successfully demonstrated in our previous works on the β-CD inclusion complexes with TCAs (Aree, 2020a, 2020b, 2020c, 2021). As noted in Section 3.2, in the solid state the 2:2 β-CD–STL HCl (**1**) and 2:2 β-CD–FXT HCl (**2**) inclusion complexes comprised two pseudo-monomeric units of which the two drug molecules were quite different. Therefore, the energy minimization by DFT method was carried out for each monomeric complex to evaluate the sole host–guest interactions necessary for the stabilization of the β-CD–STL/FXT complexes. Before the calculation, the underestimated X-ray-derived X–H bond lengths in the 1:1 β-CD–STL base and 1:1 β-CD–FXT base inclusion complexes were normalized to neutron hydrogen distances: C–H, 1.083 Å; N–H, 1.009 Å; and O–H, 0.983 Å (Allen and Bruno, 2010). The corrected structures were optimized by semiempirical PM3 method and then fully re-optimized by DFT calculation using the B3LYP functional in the gas phase with mixed basis sets 6–31+G* for H, N, O and 4-31G for C. All calculations were carried out using program GAUSSIAN09 (Frisch et al., 2009) on a DELL PowerEdge T430 server. Stabilization energy and interaction energy of the complex (ΔE_{stb} and ΔE_{int}) were calculated using Eqs. (1) and (2).

$$\Delta E_{stb} = E_{cpx} - \left(E_{\beta\text{-CD\_opt}} + E_{D\_opt}\right) \quad (1)$$

$$\Delta E_{int} = E_{cpx} - \left(E_{\beta\text{-CD\_sp}} + E_{D\_sp}\right) \quad (2)$$

where E_{cpx}, $E_{\beta\text{-CD\_opt}}$ and E_{D_opt} are the molecular energies from full-geometry optimization of complex, host β-CD and drug STL/FXT, respectively; $E_{\beta\text{-CD\_sp}}$ and E_{D_sp} are the corresponding single-point energies in the complexed states. Moreover, to assess on the extent of dimerization that helped to improve the thermodynamic stability, energy minimizations of the dimeric complexes were carried out, and the corresponding ΔE_{stb}, ΔE_{int} were evaluated (see Table S7).

3. Results and discussion

Here, we use the conventional carbohydrate nomenclature for CDs, i.e., atoms C63–O63A(B) represent the methylene C6–H_2 linked with the twofold disordered hydroxyl O6–H groups (sites A and B) of glucose residue 3 (G3) in the 2:2 β-CD–STL HCl complex (**1**), Fig. 1. Additional numbers 1 and 2 distinguish the molecular monomeric complexes β-CD–STL/FXT #1 from #2 in the triclinic asymmetric unit of both dimeric complexes **1** and **2**. Atom numbering schemes of STL HCl (**1**) and FXT HCl (**2**) are designated according to the IUPAC names, (1*S*,4*S*)-4-(3,4-dichlorophenyl)-*N*-methyl-1,2,3,4-tetrahydronaphthalen-1-amine hydrochloride and *N*-methyl-3-phenyl-3-[4-(trifluoromethyl) phenoxy]propan-1-amine hydrochloride, and further arbitrarily labeled with letters X and Y for molecular complexes #1 and #2, respectively, in the β-CD dimeric complexes. For comparison with the 2:1 β-CD–PXT base inclusion complex (Caira et al., 2003), the IUPAC name of PXT, (3*S*,4*R*)-3-[(1,3-benzodioxol-5-yloxy)methyl]-4-(4-fluorophenyl)piperidine is also adopted.

We structure the results and discussion in five sections. Sections 3.1 and 3.2 fully describe how the inclusion complexation affects the structures of β-CD macrocycles and SSRI drugs. Section 3.3 depicts the comparison of packing structures of three complexes including the 2:2 β-CD–STL, β-CD–FXT, both in triclinic, space group *P*1 and the 2:1 β-CD–PXT in monoclinic, space group $P2_1$ (Caira et al., 2003). Section 3.4 explains the structure–energy relationship established from X-ray

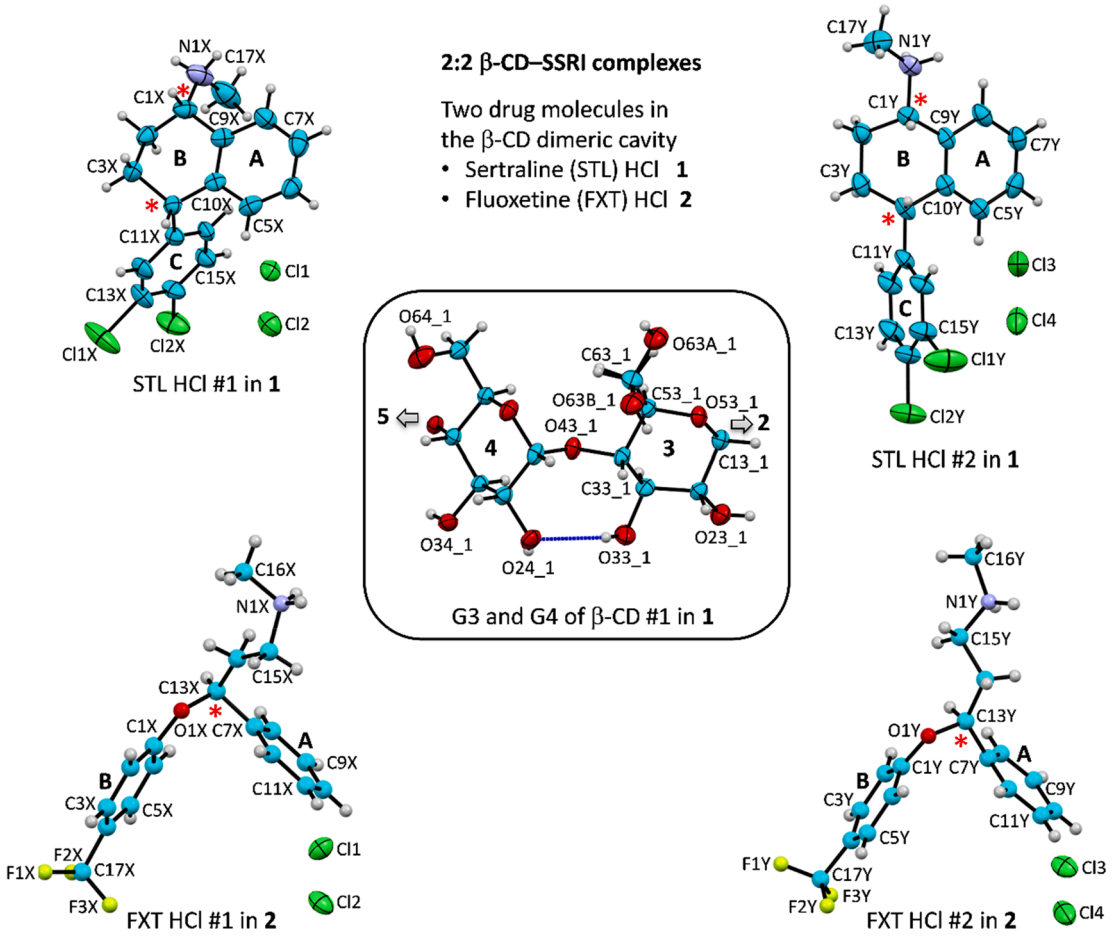

Fig. 1. Atom numbering schemes of β-CD, (1*S*,4*S*)-STL HCl and (*S*)-FXT HCl #1 and #2 in the β-CD dimeric complexes **1** and **2**; ORTEP plot at 30% probability level. The two STL and two FXT molecules are protonated at N1 and counterbalanced by doubly disordered chlorides, of which their positions are arbitrarily shown here. The chiral centers in both drugs are red starred. The connecting blue lines indicate the intramolecular, interglucose O3(n)•••O2($n+1$) hydrogen bonds stabilizing the round β-CD conformation; see also Fig. 3.

analysis combined with DFT calculation. The final Section 3.5 is devoted to the importance of SSRI conformational flexibility in their pharmacological function by comparing the structures of drugs in various lattice environments.

3.1. From TCAs to SSRIs: β-CD round structures are marginally influenced by the embedded drugs

In solution, CD inclusion complexation can take place from the uncomplexed CD hydrate, of which the water molecules residing in the CD cavity are repelled away and replaced with the hydrophobic guest. The CD macrocycle adapts its cavity to some extent to optimally accommodate partial or entire drug molecule, yielding mostly the 1:1 or 2:2 host–guest complex as frequently observed in the crystalline state (Groom et al., 2016). Here, the complexation of 2:2 β-CD–STL HCl (**1**) and 2:2 β-CD–FXT HCl (**2**) is facilitated by three factors. i) The drug molecule is rather bulky to be totally enclosed by a single CD molecule. ii) The drug molecules form dimer that is stabilized by intermolecular halogen···halogen interactions (see Sections 3.2 and 3.3). iii) The chemical nature of the least aqueous soluble native CD (β-CD) due to the more rigidity of its macrocycle and the β-CD dimer-based self-aggregates in water (Naidoo et al., 2004; Cai et al., 2008). To quantify the degree of β-CD structural adaptation upon the drug inclusion, the β-CD·12H_2O structure (Lindner and Saenger, 1982) is used as a reference structure. The CD inclusion complexation is a paradigm for the induced-fit process (Koshland, 1973) driven through weak non-covalent intermolecular interactions.

The root-mean-square (rms) deviation of structure superposition is a global parameter for quantification of the similarity of a structure pair. For CDs, the non-H atoms of CD skeleton excluding O6 are used for the calculation of rms fit. The three β-CD dimers in complex with SSRIs are non-superimposable because **1** and **2** prefer a tail-to-tail motif, while the PXT complex (Caira et al., 2003) favors a head-to-head structure (see Section 3.3). The corresponding O4-centroid–O4-centroid distances and O4 interplanar angles are 9.011 Å, 1.5°; 9.051 Å, 2.7°; and 7.000 Å, 1.2°, for **1**, **2** and the PXT complexes, respectively (Table 1 and Figs. 4, 5). The rms fit of the β-CD dimers in **1** and **2** is rather high, 1.633 Å. Therefore, the monomeric β-CD–SSRI complexes are chosen for comparison. For the 2:1 β-CD–PXT complex (Caira et al., 2003), the main β-CD #2 encapsulating the PXT piperidine moiety (A-ring) is considered (labeled i in Fig. 3a,b). Among the five β-CD molecules (**1**, **2** and i), the rms fits fall in a short range of 0.192–0.340 Å, suggesting that the round β-CDs in the three complexes are similarly affected by the inclusion of SSRI aromatic moieties (Figs. 2 and 3). Comparing to the round β-CD·12H_2O (Lindner and Saenger, 1982), the five β-CDs show larger deviations with rms fits of 0.342–0.548 Å, indicating that after complexation with the SSRI aromatic portions via C–H···π interactions, β-CDs retain a round conformation (Figs. 2 and 3). For other relevant complexes of TCA containing chlorine (clomipramine (CPM)) and tea (–)-epicatechin (EC) (Aree, 2020c; Aree and Jongrungruangchok, 2016), more distortions from the round β-CD·12H_2O (Lindner and Saenger, 1982) with respective rms fits of 0.491 and 0.562 Å are noticeable due to the large fluctuations of tilt angles and O3(n)···O2($n+1$) distances (Fig. 2a,b).

The four β-CD molecules in **1** and **2** differ mainly in the primary

Table 1
Structural parameters and inclusion geometries of two STL (**1**), two FXT (**2**) and one PXT (i) molecules embedded in the β-CD dimeric cavity.[a]

	STL#1 (**1**)	STL#2 (**1**)	FXT#1 (**2**)	FXT#2 (**2**)	PXT (i) [d]
1) Structural parameters					
Ring puckering[b]	B-ring	B-ring			D-ring
Q [Å]	0.514	0.711			0.219
θ, ϕ [°]	46.7, 153.7	91.1, 57.4			325.7
Conformation	Half chair	Boat			Envelope
Interplanar angle of two aromatic rings [°]					
A vs. C	88.5(4)	81.8(3)			
A vs. B			75.4(8)	80.5(7)	
B vs. C					9.0
Distance between ring centroids [Å]					
A – B	2.482	2.423	4.743	4.586	4.347
A – C	4.859	4.918			6.100
B – C	3.783	4.289			3.637
Selected torsion angles [°] [c]					
N1–C1–C9–C8	37.7(14)	4.2(12)			
C12–C11–C4–C10	162.4(9)	95.8(11)			
C11–C4–C10–C5	–76.7(11)	0.7(12)			
C12–C7–C13–C14			60.4(22)	81.1(27)	
C12–C7–C13–O1			–40.9(20)	–67.6(23)	
O1–C13–C14–C15			80.3(52)	–77.2(25)	
C5–C4–C18–C19					–120.5
C2–C3–C7–O8					–150.4
C7–O8–C9–C10					–9.9
2) Inclusion geometry in β-CD dimer					
Ring embedded in CD cavity	C	C	B	B	A
Interplanar angle [°]					
A-ring vs. β-CD O4 plane	56.4(3)	57.3(2)	15.2(7)	19.7(7)	72.2[h]
B/C-ring vs. β-CD O4 plane	84.7(3)	78.2(3)	64.5(5)	63.3(5)	69.3
Distance from drug to β-CD [Å]					
B/C-ring centroid to O4 centroid (diagonal)[e]	0.540	0.464	1.071	0.785	2.029
B/C-ring centroid to O4 plane (vertical)	0.399	0.360	0.906	0.668	1.640
Chiral center to O4 centroid (diagonal)[f]	–2.598	–2.682	–3.064	–3.346	–0.931
Characteristics of β-CD dimer					
Packing structure[g]	T2T		T2T		H2H
Angle between O4 planes [°]	1.5(1)		2.7(1)		1.2
O4-centroid – O4-centroid distance [Å]	9.011		9.051		7.000

[a] All SSRIs are in HCl salt form, except PXT base. For comparison to other drugs in free HCl salt form and in complex with proteins, see Table S6.
[b] Non-planar ring puckering coordinates including radius Q, azimuthal angle θ, and meridian angle ϕ (Cremer and Pople, 1975).
[c] For atom numbering, see Scheme 1.
[d] PXT base in complex with β-CD (Caira et al., 2003). All the piperidine A-rings of PXT molecules in various lattice environments adopt a normal chair form, hence the 1,3-dioxole D-ring parameters are shown here.
[e] When the β-CD O6-side pointing upwards, the positive(negative) values indicate that the A/B/C-ring centroid of a drug molecule is above(beneath) the β-CD O4 plane.
[f] Chiral centers of STL (C4), FXT (C13) and PXT (C4) are considered, see Scheme 1.
[g] Channel structure built from the asymmetric unit of β-CD dimer, tail-to-tail (T2T) and head-to-head (H2H).
[h] Plane passing through C2–C3–C5–C6 of PXT piperidine ring.

O6–H groups (excluded from the calculation of rms fit), which are flexible and oriented differently with respect to the central cavity. Only one O6–H group is disordered over two sites in **1**, while four O6–H groups are twofold disordered in **2** (Table S2). In both cases, all the O6–H groups are pointed outward the cavity with varied torsion angles χ [C4–C5–C6–O6] of 47.8–92.1° and ω [O5–C5–C6–O6] of –29.4 to –76.6° (Table S2). These O6–H groups are hydrogen bonded with the adjacent O6–H groups, water sites, and chlorides (Tables S3 and S4). Exception is O63A–H group of β-CD #1 (**1**) that is pointed toward the cavity (χ = 175.4° and ω = 55.4°), engaging in a H-bond chain of O66_1–H···O63A_1–H···O4W(O65_2), Table S3.

The origin of CD similarity is noteworthy. The CD structural parameters spring from its elemental components as follows. i) The O3(n)···O2(n + 1) distances describe the CD conformational rigidity, which is maintained by the "belt" of intramolecular, interglucose O3(n)···O2(n + 1) H-bonds. Consequently, the glucose inclination angles of a round CD structure fall into a small range. ii) The O4 glycosidic linkage related parameters include O4 deviations, O4(n)···O4(n – 1), O4(n)···centroid distances, and torsional angles ϕ [O5(n + 1)–C1(n + 1)–O4(n)–C4(n)], ψ [C1(n + 1)–O4(n)–C4(n)–C5(n)], Table S2. iii) Furthermore, for the D-glucose units composing round CDs, an ideal chair form of cyclohexane has a puckering amplitude Q = 0.63 Å and a polar angle θ = 0° (Cremer and Pople, 1975).

Given examples of the β-CD structural parameters are a) the glucose puckering parameters Q, θ; b) the tilt angles; c) the O3(n)···O2(n + 1) distances; d) the average of O4(n)···O4(n – 1)/O4(n)···centroid distance ratios (=0.868 for a perfect heptagon); and e) the sum of averages of ϕ and ψ (≈0 for closed CD structures (French and Johnson, 2007)). The corresponding values of the above parameters for **1**, **2** and [uncomplexed β-CD·12H_2O] (Lindner and Saenger, 1982) are: a) Q, 0.522–0.588 Å [0.559–0.596 Å], θ, 0.0–8.1° [1.4–7.6°]; b) 1.1–19.0° [6.4–26.2°]; c) 2.710–2.911 Å [2.770–2.957 Å]; d) 0.868–0.869 [0.870]; and e) –0.6 to –1.9° [–1.3°], Table S2. Note that the rms fits of β-CD–SSRI vs. β-CD·12H_2O are as high as 0.548 Å, which are similar to those of β-CD–EC vs. β-CD·12H_2O (0.491 Å) and β-CD–CPM vs. β-CD·12H_2O (0.562 Å). β-CDs in complex with SSRIs and TCA (CPM) (Aree, 2020c) remain round due to their small glucose inclination angles (max. 19.0° and 26.5°) and the short spans of O3(n)···O2(n + 1) distances (max. 2.911 and 2.917 Å), Table S2 and Fig. 2a,b. On the contrary, for the β-CD–EC complex (Aree and Jongrungruangchok, 2016), two opposed glucose units are tilted > 30°, giving rise to the broken belt of O3(n)···O2(n + 1) H-bonds with two O3(n)···O2(n + 1) distances > 3.2 Å.

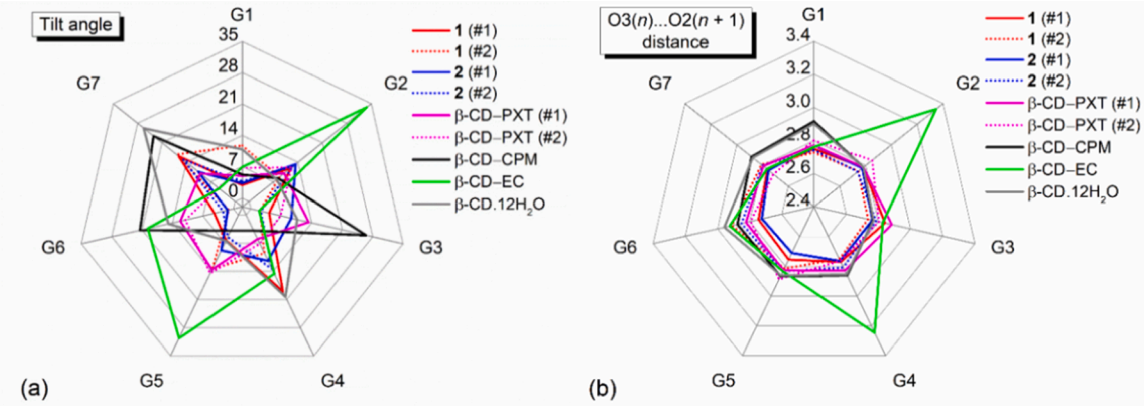

Fig. 2. Radar plots showing the variations of (a) tilt angles and (b) O3(*n*)•••O2(*n* + 1) distances of the β-CD glucose units (G1–G7) upon inclusion of SSRIs, STL HCl (**1**), FXT HCl (**2**) and PXT base (Caira et al., 2003). For comparison, data of the inclusion complexes of β-CD–(–)-epicatechin(EC) (Aree and Jongrungruangchok, 2016), β-CD–clomipramine(CPM) (Aree, 2020c) and the uncomplexed β-CD·12H_2O (Lindner and Saenger, 1982) are also incorporated; see also Table S2. Angles and distances are in ° and Å.

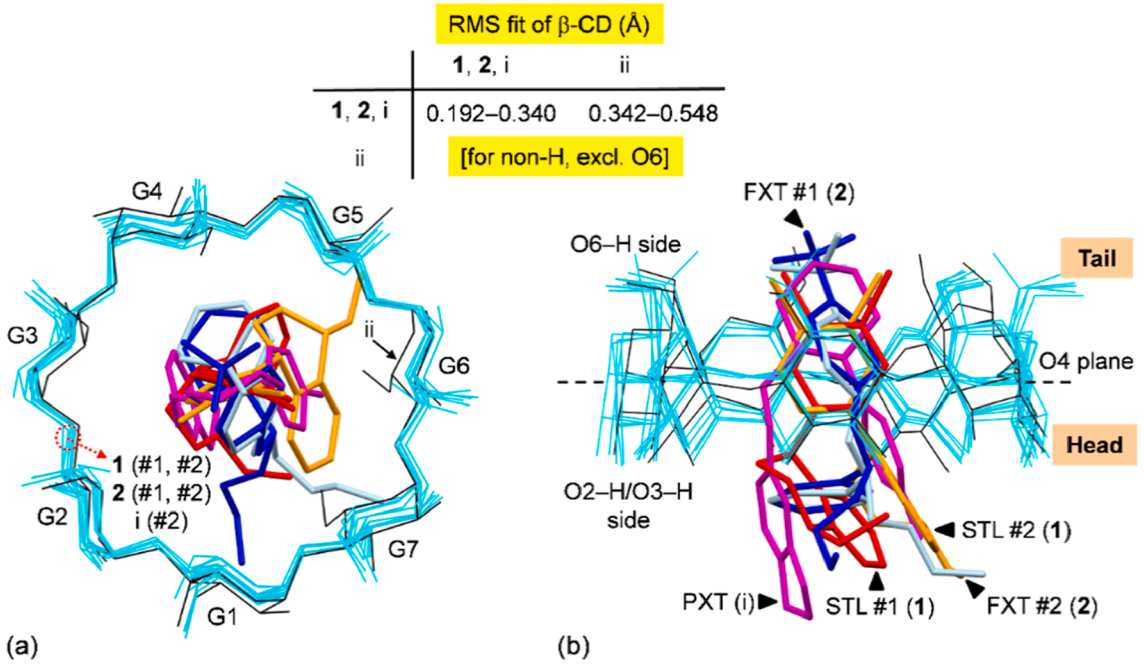

Fig. 3. Structure superpositions of the six β-CDs in complex with SSRIs (cyan wireframes), β-CD–STL #1, #2 (**1**), β-CD–FXT #1, #2 (**2**), β-CD–PXT with the main host of β-CD #2 (i; Caira et al., 2003), and in the uncomplexed β-CD·12H_2O (black wireframe, ii; Lindner and Saenger, 1982), viewed from (a) the top and (b) the side. RMS fits are computed for the host β-CDs, disregarding O6, H atoms and guests; see also Fig. 4 and Table S2.

3.2. Inclusion geometries of SSRIs in dimeric cavity and TCAs in monomeric cavity of β-CDs

SSRIs and TCAs do not share similar structural features, giving rise to their distinct pharmacological functions. Whereas TCAs possessing a [6–7-6]-tricyclic core linked with a propylamine side chain are inhibitors of both serotonin and norepinephrine, SSRIs having an aryloxypropylamine scaffold and 2–3 ring moieties are selective inhibitors of serotonin transporters (Nogrady and Weaver, 2005). The three SSRI drugs are potent for serotonin uptake in the order of PXT > STL > FXT (Stahl and Stahl, 2013). Because the β-CD encapsulation helped to improve the bioavailability of SSRIs (Passos et al. 2012; Abouhussein et al., 2019), it is worthwhile to gain atomistic insights on the β-CD–SSRI inclusion complexation.

Due to the different ring and side chain moieties of SSRIs, the varied inclusion modes of SSRIs in the β-CD cavity and the distinct host–guest stoichiometric ratios are observed in solution, β-CD–STL (Passos et al., 2011, 2013; Ogawa et al., 2015), β-CD–FXT (Ali et al., 2005; de Sousa et al., 2008) and β-CD–PXT (Bernini et al., 2004). However, crystallization nature allowed for the formation of thermodynamically favorable β-CD–SSRI complexes with a specific inclusion mode in a single crystal form. From numerous β-CD–TCA complexes with an exclusive inclusion mode of the aromatic moiety, we envisage that the SSRI aromatic moiety is also embedded in the β-CD cavity. Therefore, the relative arrangements of various components within the drug itself and with respect to the CD toroidal structure including atomistic details and intra-, intermolecular interactions are addressed using single-crystal X-ray diffraction, see below. The inherent thermodynamic stabilities of the β-CD–STL and β-CD–FXT complexes are explored in Section 3.4.

In the CD cavity, the confined guest molecule is less flexible and conformationally forced to exist in a less open structure as previously observed for the narrower butterfly angles of TCAs, of which one wing

(the aromatic A/B-ring) is enclosed in the β-CD cavity (Aree, 2020c). The flexibility of the SSRI drugs stems mainly from the non-planar six-membered B-ring of STL, the O–CH group linked the aromatic A–B-rings and the propan-1-amine side chain of FXT, and the non-planar six-membered A-ring linked the O–CH_2 group to the aromatic C-ring of PXT (Scheme 1 and Fig. 1). Therefore, the SSRI structures can be described by a number of selected torsion angles, the distances between ring centroids, and the aromatic ring interplanar angles listed for SSRIs in complex with β-CD (Table 1), and for uncomplexed SSRIs and SSRIs in complex with proteins (Table S5).

The first crystal structure of β-CD inclusion complex with SSRI (PXT base) has been reported 18 years ago (Caira et al., 2003). Here, we re-scrutinize for further insights on the structure and inclusion characteristics of PXT base enclosed in the β-CD cavity. Because PXT base is rather bulkier than other SSRIs and rather long to be hosted by a single CD, it exists in an elusive hairpin conformation stabilized by intramolecular face-to-face π···π interactions between the B- and C-rings and is encapsulated in the β-CD dimeric cavity, forming the 2:1 β-CD–PXT base complex (Caira et al., 2003). The relevant structural parameters of π···π contacts are the *Cg*(B)–*Cg*(C) distance of 3.637 Å and the interplanar angle of 9.0° (Table 1). The piperidine A-ring of PXT encapsulated in the β-CD cavity (Caira et al., 2003) adopts a normal chair form similar to other PXT in different lattice environments. By contrast, the 1,3-dioxole D-ring exist as an envelope form for PXT embedded in the β-CD cavity (Table 1) and as either a planar or an envelope structure for the PXT–protein complexes and the uncomplexed PXT (Table S5). For detailed discussion on the SSRI flexibility, see Section 3.5.

Regarding the PXT arrangement in the β-CD dimeric cavity, the PXT 1,3-benzodioxole (D–C-rings) and fluorophenyl (B-ring) moieties respectively occupy the cavity of β-CD #1 and the intra-dimer interstices, and the piperidine A-ring is situated around the O6–H side of β-CD #2 (Fig. 4 c). The A-ring (plane passing through C2–C3–C5–C6) and the B-ring make angles of 72.2 and 69.3° against the O4 plane of β-CD #2; the chiral center C4 is 0.931 Å beneath the O4 plane (Fig. 4c). Note that the 1,3-dioxole D-ring of PXT embedded in the β-CD cavity is puckered in an envelope conformation (Caira et al., 2003), whereas PXT in complex with the serotonin transporter (SERT) proteins has the 1,3-dioxole moiety in a planar geometry (Coleman and Gouaux, 2018), Tables 1 and S5. The structural distinction can be attribute to the 1,3-benzodioxole moiety that has large amplitude out-of-plane vibrations, of which 1,3-dioxole can exist as either a puckered form or a planar geometry with a small energy barrier of 0.36 kcal mol^{-1} (Emanuele and Orlandi, 2005). One PXT molecule is totally enclosed in the β-CD dimeric cavity and is maintained in position by host–guest

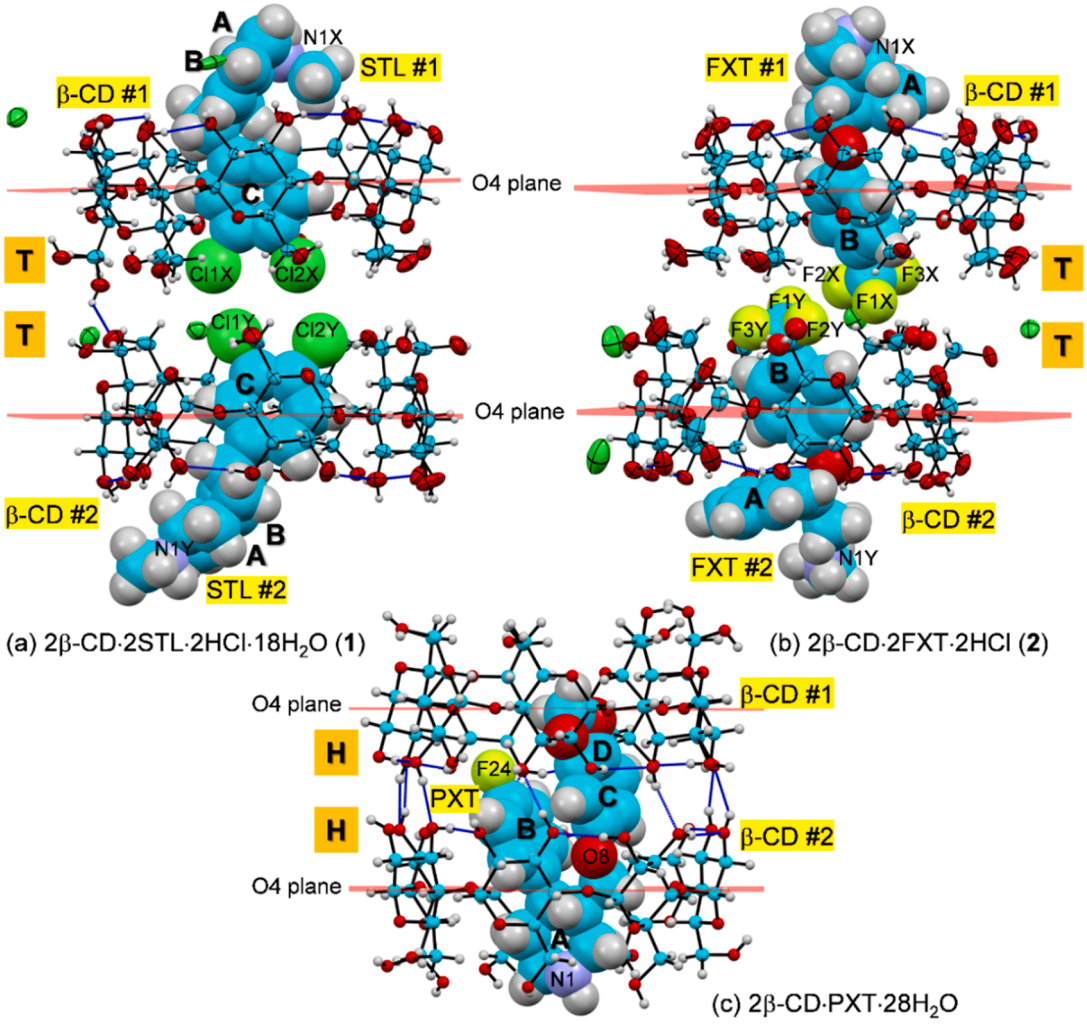

Fig. 4. β-CD dimer harboring SSRI drugs, two (1*S*,4*S*)-STL HCl (**1**), two (*S*)-FXT HCl (**2**), and one (3*S*,4*R*)-PXT base (Caira et al., 2003) in the crystalline state. ORTEP diagrams drawn at 30% probability level. For better visibility, the drug molecules are displayed in space-filling model. The twofold disordered chlorides for net charge balancing the protonated STL/FXT are shown, but the water molecules are excluded for clarity. The O–H•••O hydrogen bonds within β-CD dimer are shown with blue connecting lines. Note the distinct β-CD dimeric units are built from the different arrangements of tail-to-tail (T2T) in **1**, **2** and head-to-head (H2H) in β-CD–PXT complex (Caira et al., 2003).

Table 2
Selected host–guest interactions in 2:2 β-CD–STL HCl (**1**), 2:2 β-CD–FXT HCl (**2**) complexes in comparison with 2:1 β-CD–PXT base complex.

Interaction	D–H	H···A	D···A	∠(DHA)	Interaction	D–H	H···A	D···A	∠(DHA)
β-CD−STL HCl (**1**)					β-CD−FXT HCl (**2**)				
N1X–H1···O31_2 [i a]	0.89	1.86	2.73(1)	167.9	N1X–H1···O33_2[i]	0.89	2.500	3.24(2)	140.3
O24_1–H···N1Y [i]	0.82	2.54	3.09(1)	125.5	N1Y–H1···O24_1 [ii]	0.89	2.680	3.53(2)	161.3
N1Y–H1···O34_1 [ii]	0.89	1.96	2.83(1)	168.4	C57_1–H···*Cg*1X[c]	0.98	3.764	4.721	166.4
C54_1–H···*Cg*2X[b]	0.98	3.773	4.681	155.4	C34_1–H···*Cg*2X	0.98	3.678	4.580	154.2
C55_1–H···*Cg*2X	0.98	3.730	4.679	163.9	C57_2–H···*Cg*1Y	0.98	3.538	4.500	167.6
C54_2–H···*Cg*2Y	0.98	3.710	4.657	163.4	C34_2–H···*Cg*2Y	0.98	3.745	4.638	152.8
C36_2–H···*Cg*1Y	0.98	3.506	4.142	124.6	F2X···F1Y			2.76(3)	
C37_2–H···*Cg*1Y	0.98	3.505	4.407	154.0	β-CD−PXT base (i)[d]				
Cl1X···Cl1Y			3.87(1)		O63_1–H···N1 [iii]	0.99	1.863	2.846	169.3
Cl2X···Cl2Y			4.15(1)		N1–H···O53_1 [iv]	1.02	2.534	3.172	120.5
					C36_1–H···*Cg*1[e]	1.00	3.628	4.519	149.6
					C37_1–H···*Cg*1	1.00	3.685	4.641	160.6
					C35_2–H···*Cg*2	1.00	3.717	4.620	151.5
					C36_2–H···*Cg*2	1.00	3.262	4.248	168.4

[a]Equivalent positions: (i) *x*, *y*, *z* + 1; (ii) *x*, *y*, *z* – 1; (iii) –*x* + 2, y – 0.5, –*z* + 2; (iv) –*x* + 2, y + 0.5, –*z* + 2.
[b]STL #1: *Cg*1X = A-ring (C5X–C6X–C7X–C8X–C9X–C10X), *Cg*2X = C-ring (C11X–C12X–C13X–C14X–C15X–C16X).
STL #2: *Cg*1Y = A-ring (C5Y–C6Y–C7Y–C8Y–C9Y–C10Y), *Cg*2Y = C-ring (C11Y–C12Y–C13Y–C14Y–C15Y–C16Y).
[c]FXT #1: *Cg*1X = B-ring (C1X–C2X–C3X–C4X–C5X–C6X), *Cg*2X = A-ring (C7X–C8X–C9X–C10X–C11X–C12X).
FXT #2: *Cg*1Y = B-ring (C1Y–C2Y–C3Y–C4Y–C5Y–C6Y), *Cg*2Y = A-ring (C7Y–C8Y–C9Y–C10Y–C11Y–C12Y).
[d]Caira et al. (2003).
[e]PXT: *Cg*1 = C-ring (C9–C10–C11–C12–C16–C17), *Cg*2 = B-ring (C18–C19–C20–C21–C22–C23).

O63–H···N1–H···O53 hydrogen bonds and C3–H···π interactions (Fig. 4c and Table 2). The head-to-head β-CD dimer is stabilized by intermolecular O2–H_1/O3–H_1···O2–H_2/O3–H_2 hydrogen bonds (Caira et al., 2003).

The inclusion scenarios in the 2:2 β-CD–STL (**1**) and 2:2 β-CD–FXT (**2**) are somewhat different from what observed in the 2:1 β-CD–PXT (Caira et al., 2003). The two STL and two FXT molecules of each complex are similarly included in the β-CD dimeric cavity (Fig. 4a,b). The drug molecules insert their halogen-containing aromatic ring (STL C-ring and FXT B-ring) from the β-CD wider O2–H/O3–H side and make angles of 81.5° and 63.9° (averages) against the O4 plane. They are shifted up by 0.502 and 0.928 Å above the O4 plane (averages of ring centroid–O4 centroid distances), permitting the halogen atoms of the two encapsulated molecules to come into contact with each other, Figs. 4, 5 and Table 2. Consequently, the STL A–B-rings (**1**) and the FXT A-ring connected to propan-1-amine side chain (**2**) are located outside the cavity, nearby the O2–H/O3–H side. In both complexes, apart from the guest–guest halogen···halogen interactions, the two drug molecules are kept in position by the interplay of host–guest O2–H···N1–H···O3 H-bonds and C3/C5–H···π interactions (Figs. 4, 5 and Table 2). Similar inclusion modes are observed for the β-CD–TCA complexes (Aree, 2020a, 2020b, 2020c, 2021). The TCA aromatic A/B-rings are mostly vertically aligned in the β-CD cavity (83.7–89.7°) and their centroids are 0.467–1.384 Å above the CD molecular plane. The STL and FXT halogen moieties are encapsulated in the β-CD carrier cavity as they are bound to the transporter pocket (Zhou et al., 2009), thus maintaining the SSRI specificity for SERT (Butler and Meegan, 2008).

The distinction of the two drug molecules in **1** and **2** deserves further discussion. The two drug molecules cannot be superimposed because their relative arrangements of the structural moieties are rather different. Therefore, the more rigid portions of STL (atoms C1–C16) and FXT (atoms C1–C13 and O1) are used for the calculation, giving the respective rms fits of 0.936 and 0.212 Å (Fig. 7a,b). The greater difference between STL #1 and #2 (**1**) is due to the distinct B-rings existing in the half chair and boat conformations, respectively (Figs. 4a, 5a, 6a and Table 1). This gives rise to the differences of the B-centroid–C-centroid distance and torsion angle C12–C11–C4–C10: 3.783 Å, –76.7° for **1** and 4.289 Å, 0.7° for **2** (Table 1). By contrast, FXT #1 and #2 (**2**) excluding the propan-1-amine side chain are more similar, as indicated by the A-centroid–B-centroid distance and torsion angle C12–C7–C13–O1: 4.743 Å, –40.9° for **1** and 4.586 Å, –67.6° for **2** (Table 1). Note that starting from the racemic mixture of (*S*)- and (*R*)-FXT HCl, after the β-CD encapsulation and crystallization, the final product is the 2:2 β-CD–(*S*)-FXT inclusion complex, indicating the stronger intermolecular interactions and the enantioselective power of β-CD with the (*S*)- over the (*R*)-enantiomers. This result agrees with the enantioseparation by high performance liquid chromatography and capillary electrophoresis using β-CD phenyl isocyanate (Yu et al., 2002) and trimethyl-β-CD (Cârcu-Dobrin et al., 2017) as chiral stationary phases, respectively.

3.3. 3D-arrangements of β-CD–SSRI vs. β-CD–TCA complexes

TCAs adopt a butterfly-like shape and have a pseudo-reflection symmetry with a mirror plane bisecting the central C-ring, i.e., both wings (the aromatic A- and B-rings) are the same. Crystallographic evidence revealed that the 1:1 β-CD–TCA inclusion complexes with the TCA aromatic A/B-ring enclosed in the CD cavity exist exclusively in the orthorhombic, space group $P2_12_12_1$; β-CDs are arranged in the head-to-tail column structure (Aree, 2020a, 2020b, 2020c, 2021). The crystal lattices of β-CD complexes with six TCAs (nortriptyline, amitriptyline, desipramine, imipramine, doxepin and maprotiline) are stabilized by the unison of host–guest N–H···O, C/O–H···π, host–host O–H···O, and guest–guest edge-to-face π···π interactions (Aree, 2020a, 2020b, 2020c, 2021). On the contrary, without the guest–guest edge-to-face π···π interactions, the β-CD–protriptyline complex in the monoclinic, space group $P2_1$ favors a herringbone structure (Aree, 2021). Moreover, in the presence of chlorine in CPM, the crystal of β-CD–CPM complex is further stabilized by host–guest O–H···Cl interactions (Aree, 2020c).

The non-symmetric, more bulkier SSRIs induce the formation of β-CD dimers to encapsulate their structures, attaining more energetically favorable 2:2 β-CD–STL/FXT (**1** and **2**) and 2:1 β-CD–PXT inclusion complexes and crystallizing in the less symmetric triclinic, *P*1 and monoclinic, $P2_1$ (Caira et al., 2003), respectively. Note that the intermolecular π···π interactions between the adjacent A-rings of STL (**1**) and FXT (**2**) along the *c*-axis are facilitated by the STL conformational adaptation (boat and half chair) and by the chiral selection of (*S*)-FXT. In **1** and **2**, the tail-to-tail (T2T) β-CD dimers are stacked like a column, yielding a channel-type structure stabilized by intermolecular

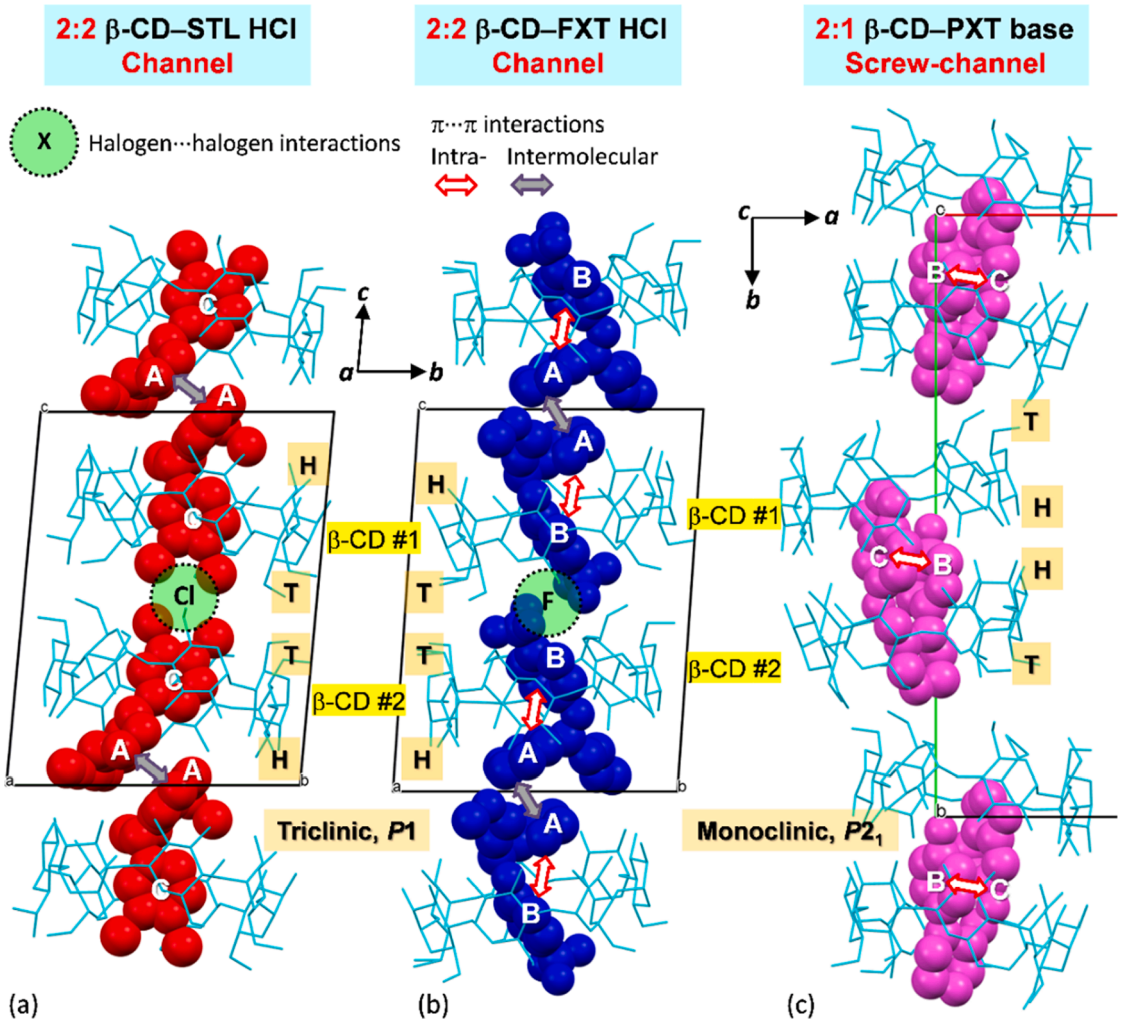

Fig. 5. 3D arrangements of the inclusion complexes (a) 2:2 β-CD–STL HCl in triclinic, *P*1 (**1**), (b) 2:2 β-CD–FXT HCl in triclinic, *P*1 (**2**), both existing in the tail-to-tail (T2T) channel structure, and (c) 2:1 β-CD–PXT base in monoclinic, $P2_1$, packing in the head-to-head (H2H) screw-channel structure (Caira et al., 2003). β-CD macrocycles, STL, FXT and PXT molecules are shown with cyan wireframes, red, blue, and magenta space-filling models, respectively. Water molecules, chlorides and H-atoms are omitted for clarity. The crystal lattices are stabilized not only by O–H•••O H-bonds within and between β-CD dimers, but also by intra-, intermolecular π•••π and halogen···halogen interactions.

halogen···halogen interactions, O6···O6 H-bonds (intradimer) and face-to-face π···π interactions, N/O–H···O/N H-bonds (interdimer), Fig. 5a,b and Tables 2, S3, S4. The halogen···halogen interactions, a class of halogen bonds, play an important role in biomolecules (Auffinger et al., 2004; Scholfield et al., 2013).

In the 2:1 β-CD–PXT complex (Caira et al., 2003), the head-to-head (H2H) β-CD dimers are stacked along twofold screw axis, parallel to the *b*-axis, giving rise to a screw-channel style stabilized by intermolecular O2/O3···O2/O3 H-bonds (intradimer) and O6···O6, N/O–H···O/N H-bonds (interdimer), Fig. 5c and Table 2. Note that the absence of intermolecular halogen···halogen interactions from the PXT complex is due to the entire inclusion of PXT fluorophenyl in the β-CD dimeric cavity; fluorine atoms are nearby the O2–H/O3–H side and have no intermolecular interaction (Caira et al., 2003).

3.4. Structures and thermodynamic stabilities of the β-CD–SSRI inclusion complexes

Weak intermolecular interactions including van der Waals, π•••π and hydrogen bond interactions are vital for the formation and maintaining the thermodynamic stability of the CD inclusion complexes. Due to the high conformational flexibility and the varied structural components of SSRI drugs, it is worthwhile to evaluate the inherent thermodynamic stabilities of the β-CD–SSRI inclusion complexes directly derived from X-ray analysis, as demonstrated here for both monomeric and dimeric β-CD–STL/FXT complexes. The neutral SSRIs in complex with β-CD in the gas phase are sufficient to give meaningful results as successfully established in the β-CD–TCA inclusion complexes (Aree, 2020a, 2020b, 2020c, 2021). For the drugs without or with one H-bond donor and a few H-bond acceptors like SSRIs and TCAs, their complexes with β-CD are primarily stabilized by host–guest C–H···π interactions. These weak intermolecular interactions contribute to the stabilization and interaction energies (ΔE_{stb} and ΔE_{int}) of –7.99 to –17.37, –8.60 to –20.93 kcal mol^{-1} for β-CD–SSRI (Table S7) and –4.22 to –8.37, –6.10 to –14.35 kcal mol^{-1} for β-CD–TCA (Aree, 2020a, 2020b, 2020c, 2021).

Because the four monomeric β-CD–STL and β-CD–FXT #1, #2 inclusion complexes share the main moiety of drug (aromatic ring) that is embedded in the β-CD cavity, they are commonly maintained in position by intermolecular C–H···π interactions (Fig. 6). Further host–guest O3–H···N1X/N1Y interactions are established via the half-chair conformation of the B-ring of STL #1 and the propan-1-amine side chain of FXT #2. These intermolecular interactions yield the more energetically favorable complexes of β-CD–STL #1 and β-CD–FXT #2 with relative stabilization energies ($\Delta\Delta E_{stb}$) of 3.19 and 9.12 kcal mol^{-1} compared to the other monomeric complexes (Figs. 6, 1S and Tables S6, S7). From monomeric to dimeric complexes, the 2:2 β-CD–STL and 2:2

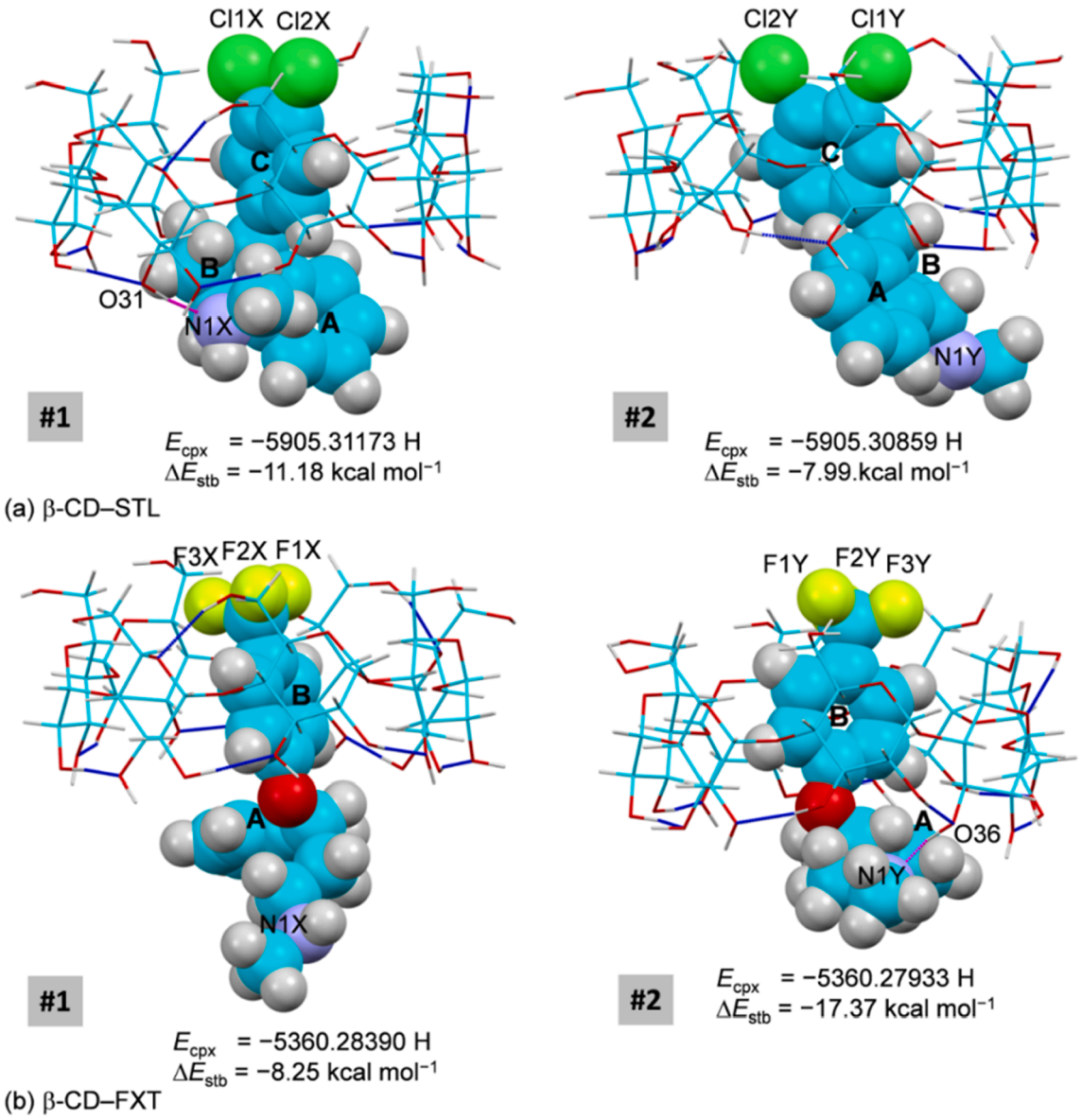

Fig. 6. Inclusion complexes of (a) β-CD−STL base and (b) β-CD−FXT base monomers #1 and #2 derived from DFT full-geometry optimization in the gas phase. For better comparison, the energy of complex (E_{cpx}) and stabilization energy (ΔE_{stb}) are given; see also Fig. S1 and Tables S6, S7. The O–H•••O H-bonds within β-CD and host–guest O–H•••N H-bonds are indicated by blue and magenta connecting lines, respectively.

β-CD–FXT complexes gain thermodynamic stability (ΔE_{stb}) by –14.50 and –20.22 kcal mol^{-1}, respectively (Table S7). The dimeric β-CD–FXT complex is 5.72 kcal mol^{-1} more energetically stable than the dimeric β-CD–STL complex because the former is stabilized by intermolecular F···F and O–H···N H-bond interactions, whereas the latter is maintained by intermolecular Cl···Cl interactions (Table S7). By contrast, the β-CD–PXT complex has a different host–guest stoichiometric ratio of 2:1, allowing one β-CD dimer to encapsulate one hairpin-like PXT molecule with self π···π interactions, without halogen···halogen interactions (Caira et al., 2003).

3.5. *Conformational flexibility of SSRIs and their pharmacological activity*

Previously, we point out that TCAs (particularly CPM) exhibit conformational flexibility while they are bound to protein binding pockets for their pharmacological activity (Aree, 2020c). Because SSRIs are much more flexible than TCAs, it is worthwhile to gain further insights into to what extent SSRIs adapt their structures for complexation with proteins, in comparison to the drugs in uncomplexed form and in the carrier (CD) cavity. To achieve the insightful comparison, the atomic coordinates of relevant structures are retrieved from the Cambridge Crystallographic Data Center (CCDC; www.ccdc.cam.ac.uk; Groom et al., 2016) and the RCSB Protein Data Bank (RCSB PDB; www.rcsb.org; Rose et al., 2015). Because the STL (1*S*,4*S*)-diastereomer, the FXT (*S*)-enantiomer and the PXT (3*S*,4*R*)-enantiomer are pharmaceutically active and included in the β-CD cavity, these structures are selected for the comparison. Due to the rather flexible SSRIs, the non-H atoms of the rigid portions are used for the calculation of rms fits, i.e., C1–C16 for (1*S*,4*S*)-STL, C1–C13, O1 for (*S*)-FXT, and N1–C6, C18–C23 for (3*S*,4*R*)-PXT (Fig. 7a,b,c). If all SSRI non-H atoms are included in the calculation, the rms fits are several times larger and increased to ~ 3 Å. The structural comparisons described below indicate the SSRI conformational changes induced each other by SERT for optimal binding with the pocket therein (Tavoulari et al., 2009).

STL HCl #2 in the β-CD cavity (**1**), STL HCl form I (Caruso et al., 1999), form II (Ravikumar et al., 2006), STL freebase (He et al., 2010) are similar with rms fits in the range 0.421–0.524 Å (Fig. 7a). STL HCl

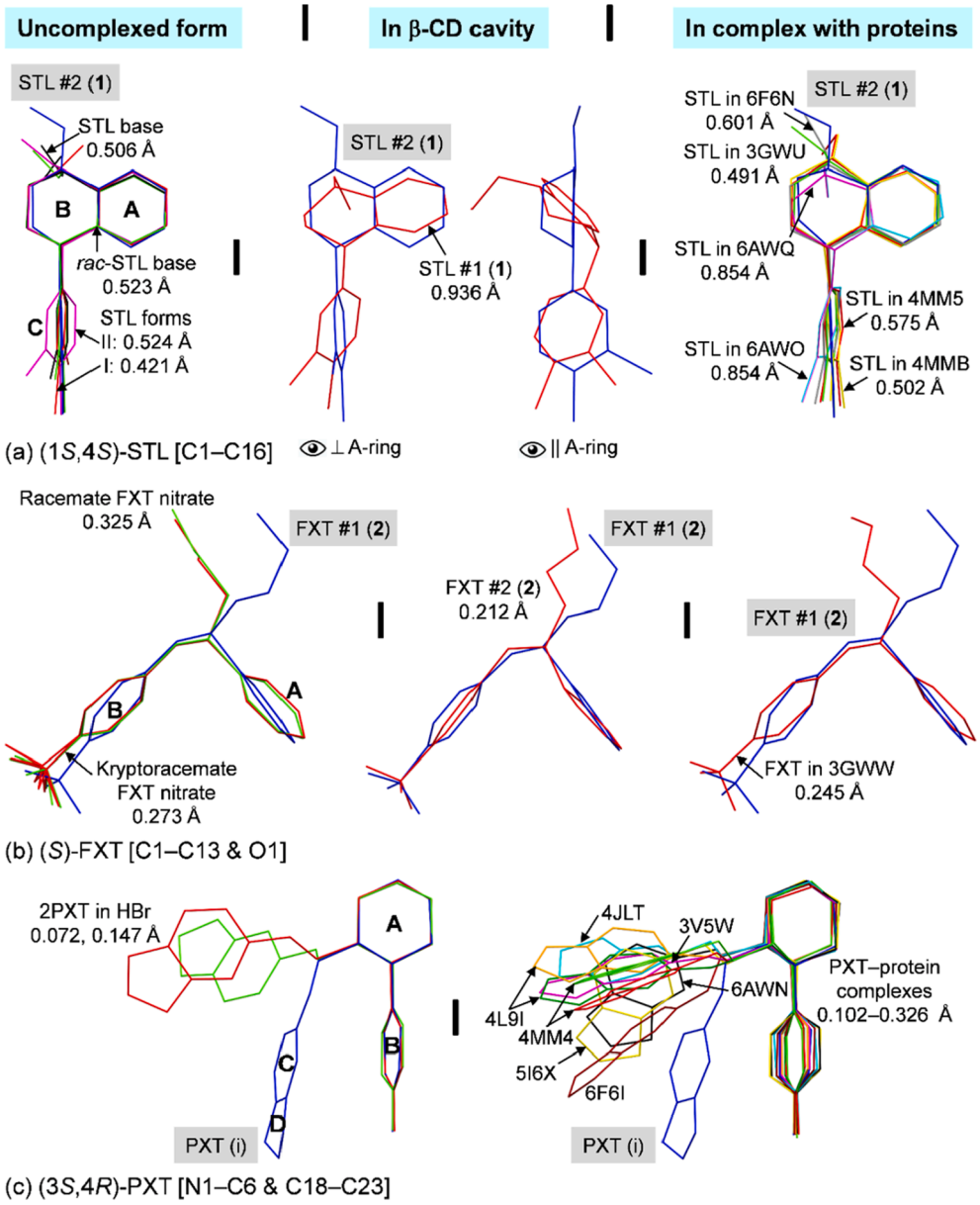

Fig. 7. Structure overlays of three SSRIs, (a) (1*S*,4*S*)-STL, (b) (*S*)-FXT and (c) (3*S*,4*R*)-PXT, in uncomplexed form, in β-CD cavity and in complex with various proteins (partitioned by |). Reference structures in (a)–(c) are shown in blue sticks of which their names are marked in gray areas and only rigid portions of drugs [in square brackets] are used for calculating the rms fits (see atom numbering in Scheme 1). The corresponding rms fit for each structure pair is indicated by nearby distance.

#1 and #2 embedded in the β-CD dimeric cavity (**1**) are rather different, rms fit 0.936 Å. This is due mainly to the distinct B-ring conformations, i.e., half chair vs. boat forms, as discussed in Section 3.2. On the contrary, a greater span of rms fits (0.491–0.854 Å) is observed when STL HCl #2 (**1**) is compared to other STL molecules in various protein binding sites including bacterial leucine transporter (LeuT; Zhou et al., 2009), human leucine biogenic leucine transporter (LeuBAT; Wang et al., 2013), human serotonin transporter (SERT; Coleman and Gouaux, 2018), and ebolavirus glycoprotein (Ren et al., 2018), Fig. 7a. Obviously, STL in complex with SERT (Coleman and Gouaux, 2018) is most distinct from STL encapsulated in the CD cavity for its optimal binding to protein and pharmacological function. This is indicated by differences in structural parameters listed in Table S5a. The B–C ring centroid distance and torsion angle C11–C4–C10–C5 are 3.865 Å, –70.7° for the SERT–STL complex (Coleman and Gouaux, 2018), and 4.122–4.287 Å, –33.8° to –47.9° for the uncomplexed STL and STL in complex with other proteins.

For FXT disregarding the propan-1-amine side chain, FXT nitrate (Carvalho et al., 2016a), FXT entrapped in carrier cavity (**2**) and FXT bound to LeuT protein (Zhou et al., 2009), FXT molecules in varied lattice environments are similar with small rms fits, 0.212–0.325 Å (Fig. 7b). The corresponding structural parameters including the A vs. B rings interplanar angle, the A–B ring centroid distance and torsion angle C12–C7–C13–O1 are: 78.0°, 4.665 Å, –54.3° for FXT–β-CD (average) and 83.8–86.0°, 5.015–5.081 Å, –16.6° to –46.8° for others (Tables 1 and S5b).

Considering merely the PXT phenylpiperidine moiety (A–B-rings), one PXT base embedded in the β-CD dimeric cavity (Caira et al., 2003), two PXT in HBr salt form (Carvalho et al., 2016b), and several PXT in complex with various proteins including LeuBAT (Wang et al., 2013), SERT (Coleman et al., 2016; Coleman and Gouaux, 2018), cytochrome P450 2B4 (Shah et al., 2013), human G protein-coupled receptor kinase (Thal et al., 2012; Homan et al., 2014), and ebolavirus glycoprotein (Ren et al., 2018) are all similar with rms fits of 0.072–0.326 Å (Fig. 7c). Note that PXT HBr·0.5H_2O (Carvalho et al., 2016b) is considered because it is

isostructural to PXT HCl·0.5H_2O (Ibers, 1999) and more accurately determined. The structural parameters including the B vs. C rings interplanar angle, the A–B, A–C ring centroid distances and torsion angle C7–O8–C9–C10 are: 9.0°, 4.347, 6.100 Å, –9.9° for the PXT– β-CD complex; and 42.3–77.3°, 4.220–4.415, 5.957–6.406 Å, –36.1° to –173.4°, 19.5–170.5° for others (Tables 1 and S5c). Note that the 1,3-benzodioxole moiety (C–D-rings) connected to CH_2–O group makes the difference among various PXT, in addition to the distinct D-ring conformations, planar vs. envelope forms (discussed in Section 3.2).

4. Conclusions

Depression, a global mental illness, became considerably worse due to the COVID-19 pandemic. Selective serotonin reuptake inhibitors (SSRIs) are first-line medications to effectively treat depression. SSRIs are equipotent to the classical drugs, tricyclic antidepressants (TCAs), but have fewer side effects. Cyclodextrins (CDs) are encapsulating agents for reducing side effects and improving drug bioavailability. Because SSRIs have variances in molecular constituents and structures without internal symmetry, their complexes with CDs and experimental findings concerning host–guest stoichiometric ratios, inclusion structures and intermolecular interactions are still rather controversial and lack the atomic details. We therefore complete an integrated structural chemistry study through single-crystal X-ray diffraction and DFT full-geometry optimization of the β-CD–SSRI inclusion complexation. Here, we demonstrate the β-CD encapsulation of sertraline (STL) HCl (**1**) and fluoxetine (FXT) HCl (**2**), in comparison to the reported complex of paroxetine (PXT) base (Caira et al., 2003).

Returning to the hypotheses posed in the introduction, it is now possible to state that X-ray analysis revealed the 2:2 β-CD–STL/FXT complexes with two drug molecules inserting their halogen-bearing aromatic ring in the β-CD dimeric cavity. **1** and **2** are stabilized by the interplay of intermolecular O2–H···N1–H···O3 H-bonds, C3/C5–H···π and halogen···halogen interactions. Similarly, the 1:1 β-CD–TCA complexes with an exclusive inclusion mode of the aromatic ring are maintained by C3/C5–H···π interactions (Aree, 2020a, 2020b, 2020c, 2021). On the other hand, the 2:1 β-CD–PXT complex with a total inclusion is stabilized by host–guest O6–H···N1–H···O5 H-bonds and C3/C5–H···π interactions (Caira et al., 2003). The inherent stabilization energies of both complexes evaluated using DFT energy-minimization in vacuum suggest the improved thermodynamic stabilities of drugs upon CD inclusion complexation. Moreover, the SSRI conformational flexibilities facilitate their pharmacological functions, as perceived from the insightful structural comparison of the drugs in free salt form, in carrier (CD) cavity and in complex with proteins. This work has gone a long way toward advancing our understanding at atomic level of the β-CD encapsulation of antidepressants for an effective application of CDs in drug delivery system. The continuation study on other two key SSRIs, citalopram, and escitalopram (the most selective SSRI), is in progress, providing an integral picture of the β-CD–SSRI inclusion complexation in the coming future.

CRediT authorship contribution statement

Thammarat Aree: Funding acquisition, Conceptualization, Methodology, Formal analysis, Writing– original draft, Writing – review & editing.

Declaration of Competing Interest

The authors declare that they have no known competing financial interests or personal relationships that could have appeared to influence the work reported in this paper.

Acknowledgements

This research was made possible by a grant from the Ratchadapisek Sompoch Endowment Fund, Chulalongkorn University (RCU_H_64_031_23).

Appendix A. Supplementary material

Supplementary data to this article can be found online at https://doi.org/10.1016/j.ijpharm.2021.121113.

References

Abouhussein, D.M.N., El Nabarawi, M.A., Shalaby, S.H., El-Bary, A.A., 2019. Sertraline-cyclodextrin complex orodispersible sublingual tablet: optimization, stability, and pharmacokinetics. J. Pharm. Inno. 16 (1), 53–66. https://doi.org/10.1007/s12247-019-09416-1.

Adeoye, O., Cabral-Marques, H., 2017. Cyclodextrin nanosystems in oral drug delivery: a mini review. Int. J. Pharm. 531 (2), 521–531. https://doi.org/10.1016/j.ijpharm.2017.04.050.

Ali, S.M., Asmat, F., Maheshwari, A., Koketsu, M., 2005. Complexation of fluoxetine hydrochloride with β-cyclodextrin. A proton magnetic resonance study in aqueous solution. Il Farmaco 60 (5), 445–449. https://doi.org/10.1016/j.farmac.2005.03.003.

Allen, F.H., Bruno, I.J., 2010. Bond lengths in organic and metal-organic compounds revisited: X—H bond lengths from neutron diffraction data. Acta Cryst. B66, 380–386. https://doi.org/10.1107/S0108768110012048.

Aree, T., Jongrungruangchok, S., 2016. Crystallographic evidence for β-cyclodextrin inclusion complexation facilitating the improvement of antioxidant activity of tea (+)-catechin and (−)-epicatechin. Carbohydr. Polym. 140, 362–373. https://doi.org/10.1016/j.carbpol.2015.12.066.

Aree, T., 2020a. β-Cyclodextrin encapsulation of nortriptyline HCl and amitriptyline HCl: molecular insights from single-crystal X-ray diffraction and DFT calculation. Int. J. Pharm. 575, 118899 https://doi.org/10.1016/j.ijpharm.2019.118899.

Aree, T., 2020b. β-Cyclodextrin inclusion complexation with tricyclic antidepressants desipramine and imipramine: a structural chemistry perspective. J. Pharm. Sci. 109, 3086–3094. https://doi.org/10.1016/j.xphs.2020.10.017.

Aree, T., 2020c. Supramolecular complexes of β-cyclodextrin with clomipramine and doxepin: effect of the ring substituent and component of drugs on their inclusion topologies and structural flexibilities. Pharmaceuticals 13, 278. https://doi.org/10.3390/ph13100278.

Aree, T., 2021. Distinctive supramolecular features of β-cyclodextrin inclusion complexes with antidepressants protriptyline and maprotiline: a comprehensive structural investigation. Pharmaceuticals 14, 812. https://doi.org/10.3390/ph14080812.

Auffinger, P., Hays, F.A., Westhof, E., Ho, P.S., 2004. Halogen bonds in biological molecules. PNAS 101 (48), 16789–16794. https://doi.org/10.1073/pnas.0407607101.

Bakshi, P.R., Londhe, V.Y., 2020. Widespread applications of host-guest interactive cyclodextrin functionalized polymer nanocomposites: Its meta-analysis and review. Carbohydr. Polym. 242, 116430. https://doi.org/10.1016/j.carbpol.2020.116430.

Belica, S., Jeziorska, D., Urbaniak, P., Buko, V.U., Zavodnik, I.B., Pałecz, B., 2014. Calorimetric and spectroscopic characterization of complexes between β-cyclodextrin or heptakis (2,6-di-O-methyl)-β-cyclodextrin and sertraline hydrochloride in aqueous solution. J. Chem. Thermodyn. 70, 160–167. https://doi.org/10.1016/j.jct.2013.10.035.

Bernini, A., Spiga, O., Ciutti, A., Scarselli, M., Bottoni, G., Mascagni, P., Niccolai, N., 2004. NMR studies of the inclusion complex between β-cyclodextrin and paroxetine. Eur. J. Pharm. Sci. 22 (5), 445–450. https://doi.org/10.1016/j.ejps.2004.04.007.

Bruker, 2008. SAINT and XPREP. Bruker AXS Inc, Madison, WI.

Bruker, 2014. APEX2, SADABS and SHELXTL. Bruker AXS Inc, Madison, WI.

Buko, V., Palecz, B., Belica-Pacha, S., Zavodnik, I., 2017. The supramolecular complex of sertraline with cyclodextrins: physicochemical and pharmacological properties. In: Nano-and Microscale Drug Delivery Systems. Elsevier, pp. 343–356. https://doi.org/10.1016/B978-0-323-52727-9.00018-2.

Butler, S.G., Meegan, M.J., 2008. Recent developments in the design of anti-depressive therapies: targeting the serotonin transporter. Curr. Med. Chem. 15, 1737–1761. https://doi.org/10.2174/092986708784872357.

Cai, W., Sun, T., Shao, X., Chipot, C., 2008. Can the anomalous aqueous solubility of β-cyclodextrin be explained by its hydration free energy alone? Phys. Chem. Chem. Phys. 10, 3236–3243. https://doi.org/10.1039/B717509D.

Caira, M.R., De Vries, E., Nassimbeni, L.R., Jacewicz, V.W., 2003. Inclusion of the antidepressant paroxetine in β-cyclodextrin. J. Incl. Phenom. Macrocycl. Chem. 46, 37–42. https://doi.org/10.1023/A:1025622809025.

Cârcu-Dobrin, Melania, Budău, Monica, Hancu, Gabriel, Gagyi, Laszlo, Rusu, Aura, Kelemen, Hajnal, 2017. Enantioselective analysis of fluoxetine in pharmaceutical formulations by capillary zone electrophoresis. Saudi Pharm. J. 25 (3), 397–403. https://doi.org/10.1016/j.jsps.2016.09.007.

Caruso, F., Besmer, A., Rossi, M., 1999. The absolute configuration of sertraline (Zoloft) hydrochloride. Acta Cryst. C55, 1712–1714. https://doi.org/10.1107/S0108270199008343.

Carvalho Jr, P.S., Ellena, J., Yufit, D.S., Howard, J.A., 2016a. Rare case of polymorphism in a racemic fluoxetine nitrate salt: phase behavior and relative stability. Cryst. Growth Des. 16, 3875–3883. https://doi.org/10.1021/acs.cgd.6b00442.

Carvalho Jr, P.S., C. de Melo, C., Ayala, A.P., da Silva, C.C., Ellena, J., 2016b. Reversible solid-state hydration/dehydration of paroxetine HBr hemihydrate: structural and thermochemical studies. Cryst. Growth Des. 16, 1543–1549. https://doi.org.10.1021/acs.cgd.5b01672.

Coleman, Jonathan A., Green, Evan M., Gouaux, Eric, 2016. X-ray structures and mechanism of the human serotonin transporter. Nature 532 (7599), 334–339. https://doi.org/10.1038/nature17629.

Coleman, Jonathan A., Gouaux, Eric, 2018. Structural basis for recognition of diverse antidepressants by the human serotonin transporter. Nat. Struct. Mol. Biol. 25 (2), 170–175. https://doi.org/10.1038/s41594-018-0026-8.

Cremer, D., Pople, J.A., 1975. General definition of ring puckering coordinates. J. Am. Chem. Soc. 97 (6), 1354–1358. https://doi.org/10.1021/ja00839a011.

Del Valle, E.M., 2004. Cyclodextrins and their uses: a review. Process Biochem. 39 (9), 1033–1046. https://doi.org/10.1016/S0032-9592(03)00258-9.

Diniz, T.C., Pinto, T.C.C., Menezes, P.D.P., Silva, J.C., Teles, R.B.D.A., Ximenes, R.C.C., ... Almeida, J.R.G.D.S., 2018. Cyclodextrins improving the physicochemical and pharmacological properties of antidepressant drugs: a patent review. Expert Opin. Ther. Pat. 28, 81–92. https://doi.org/10.1080/13543776.2017.1384816.

Dodziuk, H., 2006. Cyclodextrins and their complexes: Chemistry, analytical methods, applications. Wiley-VCH, Weinheim, Germany.

Emanuele, E., Orlandi, G., 2005. Large amplitude out-of-plane vibrations of 1, 3-benzodioxole in the S_0 and S_1 states: An analysis of fluorescence and excitation spectra by ab initio calculations. J. Phys. Chem. A 109, 6471–6482. https://doi.org/10.1021/jp051055w.

Emsley, P., Lohkamp, B., Scott, W.G., Cowtan, K., 2010. Features and development of Coot. Acta Cryst. 66 (4), 486–501. https://doi.org/10.1107/S0907444910007493.

Food and Drug Administration (FDA), 2014. Selective Serotonin Reuptake Inhibitors (SSRIs) Information. https://www.fda.gov/drugs/information-drug-class/selective-serotonin-reuptake-inhibitors-ssris-information. December 23, 2014. Accessed on 11 June 2021.

Fourmentin, S., Crini, G., Lichtfouse, E. (Eds.), 2018. Cyclodextrin applications in medicine, food, environment and liquid crystals (Vol. 17). Springer.

French, Alfred D., Johnson, Glenn P., 2007. Linkage and pyranosyl ring twisting in cyclodextrins. Carbohydr. Res. 342 (9), 1223–1237. https://doi.org/10.1016/j.carres.2007.02.033.

Frisch, M.J.E.A., Trucks, G.W., Schlegel, H.B., Scuseria, G.E., Robb, M.A., Cheeseman, J. R., ... Nakatsuji, H. 2009. GAUSSIAN09, Revision A.01. Gaussian. Inc., Wallingford, CT.

Géczy, J., Bruhwyler, J., Scuvée-Moreau, J., Seutin, V., Masset, H., Van Heugen, J.C., Dresse, A., Lejeune, C., Decamp, E., Szente, L., Szejtli, J., Liégeois, J.-F., 2000. The inclusion of fluoxetine into γ-cyclodextrin increases its bioavailability: behavioural, electrophysiological and pharmacokinetic studies. Psychopharmacol. 151 (4), 328–334. https://doi.org/10.1007/s002130000512.

Groom, C.R., Bruno, I.J., Lightfoot, M.P., Ward, S.C., 2016. The Cambridge structural database. Acta Cryst. B72, 171-179. https://doi.org/10.1107/S2052520616003954.

He, Quan, Rohani, Sohrab, Zhu, Jesse, Gomaa, Hassan, 2010. Sertraline racemate and enantiomer: solid-state characterization, binary phase diagram, and crystal structures. Cryst. Growth Des. 10 (4), 1633–1645. https://doi.org/10.1021/cg901197b.

Hoertel, N., Sánchez-Rico, M., Vernet, R., Beeker, N., Jannot, A.S., Neuraz, A., ... Limosin, F., 2021. Association between antidepressant use and reduced risk of intubation or death in hospitalized patients with COVID-19: results from an observational study. Mol. Psychiatry 26, 1–14. https://doi.org/10.1038/s41380-021-01021-4.

Homan, K.T., Wu, E., Wilson, M.W., Singh, P., Larsen, S.D., Tesmer, J.J., 2014. Structural and functional analysis of G protein–coupled receptor kinase inhibition by paroxetine and a rationally designed analog. Mol. Pharmacol. 85, 237–248. https://doi.org/10.1124/mol.113.089631.

Ibers, J.A., 1999. Paroxetine hydrochloride hemihydrate. Acta Cryst. C55, 432–434. https://doi.org/10.1107/S0108270198013444.

Koshland, D.E., 1973. Protein shape and biological control. Sci. Am. 229, 52–64. https://www.jstor.org/stable/24923220.

Lenze, Eric J., Mattar, Caline, Zorumski, Charles F., Stevens, Angela, Schweiger, Julie, Nicol, Ginger E., Miller, J. Philip, Yang, Lei, Yingling, Michael, Avidan, Michael S., Reiersen, Angela M., 2020. Fluvoxamine vs placebo and clinical deterioration in outpatients with symptomatic COVID-19: a randomized clinical trial. JAMA 324 (22), 2292. https://doi.org/10.1001/jama.2020.22760.

Lindner, Klaus, Saenger, Wolfram, 1982. Crystal and molecular structure of cycloheptaamylose dodecahydrate. Carbohydr. Res. 99 (2), 103–115. https://doi.org/10.1016/S0008-6215(00)81901-1.

Liu, Y., Chen, Y., Gao, X., Fu, J., Hu, L., 2020. Application of cyclodextrin in food industry. Crit. Rev. Food Sci. Nutr. 1–15 https://doi.org/10.1080/10408398.2020.1856035.

Lopes, J.F., Nascimento Jr, C.S., Anconi, C.P., Dos Santos, H.F., De Almeida, W.B., 2015. Inclusion complex thermodynamics: the β-cyclodextrin and sertraline complex example. J. Mol. Graph. Model. 62, 11–17. https://doi.org/10.1016/j.jmgm.2015.08.008.

McClanahan, Kimberly K., 2009. Depression in pregnant adolescents: considerations for treatment. J. Pediatr. Adolesc. Gynecol. 22 (1), 59–64. https://doi.org/10.1016/j.jpag.2008.04.006.

Meikle, Claire Kyung Sun, Creeden, Justin Fortune, McCullumsmith, Cheryl, Worth, Randall G., 2021. SSRIs: Applications in inflammatory lung disease and implications for COVID-19. Neuropsychopharmacol. Rep. 41 (3), 325–335. https://doi.org/10.1002/npr2.12194.

Morin-Crini, Nadia, Fourmentin, Sophie, Fenyvesi, Éva, Lichtfouse, Eric, Torri, Giangiacomo, Fourmentin, Marc, Crini, Grégorio, 2021. 130 years of cyclodextrin discovery for health, food, agriculture, and the industry: a review. Environ. Chem. Lett. 19 (3), 2581–2617. https://doi.org/10.1007/s10311-020-01156-w.

Naidoo, Kevin J., Chen, Jeff Yu-Jen, Jansson, Jennie L.M., Widmalm, Göran, Maliniak, Arnold, 2004. Molecular properties related to the anomalous solubility of β-cyclodextrin. J. Phys. Chem. B 108 (14), 4236–4238. https://doi.org/10.1021/jp037704q.

Nogrady, T., Weaver, D.F., 2005. Medicinal chemistry: a molecular and biochemical approach. Oxford University Press.

Ogawa, Noriko, Hashimoto, Takuro, Furuishi, Takayuki, Nagase, Hiromasa, Endo, Tomohiro, Yamamoto, Hiromitsu, Kawashima, Yoshiaki, Ueda, Haruhisa, 2015. Solid-state characterization of sertraline base–β-cyclodextrin inclusion complex. J. Pharm. Biomed. Anal. 107, 265–272. https://doi.org/10.1016/j.jpba.2014.12.036.

Our World in Data, 2021. Total confirmed COVID-19 cases. https://ourworldindata.org/grapher/covid-cases-income. Date: June 8, 2021. Accessed on 11 June 2021.

Passos, Joel J., De Sousa, Frederico B., Lula, Ivana S., Barreto, Elison A., Lopes, Juliana Fedoce, De Almeida, Wagner B., Sinisterra, Rubén D., 2011. Multi-equilibrium system based on sertraline and β-cyclodextrin supramolecular complex in aqueous solution. Int. J. Pharm. 421 (1), 24–33. https://doi.org/10.1016/j.ijpharm.2011.09.026.

Passos, Joel J., De Sousa, Frederico B., Mundim, Iram M., Bonfim, Ricardo R., Melo, Robson, Viana, Alice F., Stolz, Eveline D., Borsoi, Milene, Rates, Stela M.K., Sinisterra, Rubén D., 2012. In vivo evaluation of the highly soluble oral β-cyclodextrin–Sertraline supramolecular complexes. Int. J. Pharm. 436 (1-2), 478–485. https://doi.org/10.1016/j.ijpharm.2012.06.061.

Passos, J.J., De Sousa, F.B., Lula, I.S., Barreto, E.A., Lopes, J.F., De Almeida, W.B., Sinisterra, R.D., 2013. Corrigendum to "Multi-equilibrium system based on sertraline and β-cyclodextrin supramolecular complex in aqueous solution" [Int. J. Pharmaceut. 421 (2011) 24–33]. Int. J. Pharm. 444 https://doi.org/10.1016/j.ijpharm.2013.01.064, 201–201.

Peretti, S.J.R.H.I., Judge, R., Hindmarch, I., 2000. Safety and tolerability considerations: tricyclic antidepressants vs. selective serotonin reuptake inhibitors. Acta Psychiatr. Scand. 101, 17–25. https://doi.org/10.1111/j.1600-0447.2000.tb10944.x.

Perlis, Roy H., Ognyanova, Katherine, Santillana, Mauricio, Baum, Matthew A., Lazer, David, Druckman, James, Della Volpe, John, 2021. Association of acute symptoms of COVID-19 and symptoms of depression in adults. JAMA Netw. Open 4 (3), e213223. https://doi.org/10.1001/jamanetworkopen.2021.3223.

Ravikumar, K., Sridhar, B., Bhanu, M.N., 2006. Sertraline hydrochloride form II. Acta Cryst. E62, o565–o567. https://doi.org/10.1107/S1600536806000730.

Ren, J., Zhao, Y., Fry, E.E., Stuart, D.I., 2018. Target identification and mode of action of four chemically divergent drugs against Ebolavirus infection. J. Med. Chem. 61, 724–733. https://doi.org/10.1021/acs.jmedchem.7b01249.

Rogers, J.P., Watson, C.J., Badenoch, J., Cross, B., Butler, M., Song, J., ... Rooney, A.G., 2021. Neurology and neuropsychiatry of COVID-19: a systematic review and meta-analysis of the early literature reveals frequent CNS manifestations and key emerging narratives. J. Neurol. Neurosurg. Psychiatry. 92, 1–10. https://doi.org/10.1136/jnnp-2021-326405.

Rose, P.W., Prlić, A., Bi, C., Bluhm, W.F., Christie, C.H., Dutta, S., ... Young, J., 2015. The RCSB Protein Data Bank: views of structural biology for basic and applied research and education. Nucleic Acids Res. 43, D345–D356. https://doi.org/10.1093/nar/gku1214.

Scholfield, Matthew R., Zanden, Crystal M. Vander, Carter, Megan, Ho, P. Shing, 2013. Halogen bonding (X-bonding): A biological perspective. Protein Sci. 22 (2), 139–152. https://doi.org/10.1002/pro.2201.

Shah, Manish B., Kufareva, Irina, Pascual, Jaime, Zhang, Qinghai, Stout, C. David, Halpert, James R., 2013. A structural snapshot of CYP2B4 in complex with paroxetine provides insights into ligand binding and clusters of conformational states. J. Pharmacol. Exp. Ther. 346 (1), 113–120. https://doi.org/10.1124/jpet.113.204776.

Desousa, F., Denadai, A., Lula, I., Lopes, J., Dossantos, H., Dealmeida, W., Sinisterra, R., 2008. Supramolecular complex of fluoxetine with β-cyclodextrin: An experimental and theoretical study. Int. J. Pharma. 353 (1-2), 160–169. https://doi.org/10.1016/j.ijpharm.2007.11.050.

Spek, A.L., 2015. PLATON SQUEEZE: a tool for the calculation of the disordered solvent contribution to the calculated structure factors. Acta Cryst. C71, 9–18. https://doi.org/10.1107/S2053229614024929.

Stahl, S.M., Stahl, S.M., 2013. Stahl's essential psychopharmacology: neuroscientific basis and practical applications. Cambridge University Press.

Stokes, Peter E., Holtz, Aliza, 1997. Fluoxetine tenth anniversary update: the progress continues. Clin. Ther. 19 (5), 1135–1250. https://doi.org/10.1016/S0149-2918(97)80066-5.

Tavoulari, S., Forrest, L.R., Rudnick, G., 2009. Fluoxetine (Prozac) binding to serotonin transporter is modulated by chloride and conformational changes. J. Neurosci. 29, 9635–9643. https://doi.org/10.1523/JNEUROSCI.0440-09.2009.

Thal, David M., Homan, Kristoff T., Chen, Jun, Wu, Emily K., Hinkle, Patricia M., Huang, Z. Maggie, Chuprun, J. Kurt, Song, Jianliang, Gao, Erhe, Cheung, Joseph Y., Sklar, Larry A., Koch, Walter J., Tesmer, John J.G., 2012. Paroxetine is a direct inhibitor of g protein-coupled receptor kinase 2 and increases myocardial contractility. ACS Chem. Biol. 7 (11), 1830–1839. https://doi.org/10.1021/cb3003013.

Wang, Hui, Goehring, April, Wang, Kevin H., Penmatsa, Aravind, Ressler, Ryan, Gouaux, Eric, 2013. Structural basis for action by diverse antidepressants on biogenic amine transporters. Nature 503 (7474), 141–145. https://doi.org/10.1038/nature12648.

Wong, David T., Bymaster, Frank P., Reid, Leroy R., Fuller, Ray W., Perry, Kenneth W., 1985. Inhibition of serotonin uptake by optical isomers of fluoxetine. Drug Dev. Res. 6 (4), 397–403. https://doi.org/10.1002/(ISSN)1098-229910.1002/ddr.v6:410.1002/ddr.430060412.

World Health Organization. (WHO), 2017. Depression and Other Common Mental Disorders: Global Health Estimates URL: http://apps.who.int/iris/bitstream/10665/254610/1/WHO-MSD-MER-2017.2-eng.pdf. Accessed on 11 June 2021.

Yu, Hongwei, Ching, Chi Bun, Fu, Ping, Ng, Siu Chong, 2002. Enantioseparation of fluoxetine on a new β-cyclodextrin bonded phase column by HPLC. Sep. Sci. Technol. 37 (6), 1401–1415. https://doi.org/10.1081/SS-120002618.

Zhou, Z., Zhen, J., Karpowich, N.K., Law, C.J., Reith, M.E., Wang, D.N., 2009. Antidepressant specificity of serotonin transporter suggested by three LeuT–SSRI structures. Nat. Struct. Mol. Biol. 16 (6), 652–657. https://doi.org/10.1038/nsmb.1602.